A LARGE-AREA GAMMA-RAY IMAGING TELESCOPE SYSTEM

NASW-3743
Final Report

For the period 24 March 1983 through 1 September 1983

Principal Investigator:

David G. Koch

Prepared for:

National Aeronautics and Space Administration Headquarters
Washington, D.C. 20546

August 1983

Smithsonian Institution
Astrophysical Observatory
Cambridge, Massachusetts 02138

The Smithsonian Astrophysical Observatory
is a member of the
Harvard-Smithsonian Center for Astrophysics

A LARGE-AREA GAMMA-RAY IMAGING TELESCOPE SYSTEM

NASW-3743
Final Report

For the period 24 March 1983 through 1 September 1983

Principal Investigator:

David G. Koch

Prepared for:

National Aeronautics and Space Administration Headquarters
Washington, D.C. 20546

August 1983

Smithsonian Institution
Astrophysical Observatory
Cambridge, Massachusetts 02138

Abstract

This report details the concept definition of using the External Tank (ET) of the Space Shuttle as the basis for constructing a large-area gamma-ray imaging telescope in space. The telescope will be used to locate and study cosmic sources of gamma-rays of energy greater than 100 MeV. The report describes in detail both the telescope properties and the means whereby an ET is used for this purpose. A parallel is drawn between those systems that would be common to both a Space Station and this ET application. In addition, those systems necessary for support of the telescope can form the basis for using the ET as part of the Space Station. The major conclusions of this concept definition are that the ET is ideal for making into a gamma-ray telescope, and that this telescope will provide the substantial increase in collecting area recommended by the National Academy of Sciences. The principal recommendation is that NASA proceed at this time with a design definition of the concept presented herein.

Key words: Space Station, External Tank Applications, Telescopes, Gamma-Ray Detectors

Acknowledgements

The concept presented here is not new in its parts. The original idea for the telescope is that of Kenneth Greisen. The concept of using a spent SIVB fuel tank had been proposed as part of the Orbital Workshop, later known as Skylab. The possibility of applications of the ET has been kicking around for a number of years. Smaller versions of the telescope had been proposed as part of the HEAO and Spacelab programs. However, it wasn't until now that this has all come together along with the real need for a telescope to follow up on the work of GRO. Therefore, I appreciate all the thoughts of others that have led to this concept.

In addition to the study done at SAO, a parallel effort was performed by the Advanced Programs group of the Michoud Division of Martin Marietta Aerospace (MMA). A copy of this report is available from Frank Williams, Director Advanced Programs, Martin Marietta Aerospace, P. O. Box 29304, New Orleans, LA 70189 [(504) 255-3738]. Section 5 of this study is almost entirely drawn from the MMA IR&D report. Other details and thoughts from MMA are distributed throughout this study and it is difficult to isolate and credit each individual one. I appreciate the interest and support of this group.

The work performed for this study was supported by NASA contract NASW-3743.

A Large Area Gamma-Ray Imaging Telescope System
Final Report

Table of Contents

Illustrations and Tables

List of Acronyms and Abbreviations

ACC	aft cargo carrier
ECL	emitter coupled logic
ET	External Tank
eV	electron Volt
EVA	extravehicular activity
FOV	field of view
γ	Lorentz factor
GeV	gega electron Volts (10^9)
GRO	Gamma Ray Observatory
HEAO	High Energy Astronomy Observatory
HV	high voltage
IMU	inertial measuring unit
IR&D	Independent research and development
KSC	Kennedy Space Center
LDR	Large Deployable Reflector
MECO	Main engine cutoff
MeV	Million electron Volts
MMA	Martin Marietta Aerospace
MMU	manned maneuvering unit
MWS	mobile work station
NA	not applicable
NASA	National Aeronautics and Space Administration
OMS	orbiter maneuvering system
OSO	Orbiting Solar Observatory
PAM-D	payload assist module, delta class
PMT	photomultiplier tube
psia	pounds per square inch absolute
RCA	Radio Corporation of America
RCS	reaction control system
rms	root mean square
RMS	remote manipulator system
rss	root sum square
SAO	Smithsonian Astrophysical Observatory
SAS	Small Astronomy Satellite
SOFI	spray on foam insulation
SRB	solid rocket boosters
SSS	support system saddle
STA	station
STS	Space Transportation System
TOF	time of flight

1.0 THE CONCEPT

The advent of the Shuttle has brought with it a greatly increased capability to work in space. The Shuttle as a system was designed for reuse. The only major hardware component that is an expendable is the External Tank (ET). Presently, the ET is taken to 98% of orbital velocity and then it is disposed, since it is no longer of any use. However, the fact that it is a large, thin-walled, gas-tight, light-tight, rigid pressure vessel makes it ideally suited for use as a gamma-ray telescope. A number of studies have been conducted to find applications for the ET (Cal Space 1982). Many of the ideas proposed call for considerable on-orbit reworking of the ET (such as cutting off an end or melting it down for its value in raw materials). But for this application, the ET would be used as is, with only minor modifications in the manufacturing process to permit later attachment of hardware on-orbit. None of the modifications would necessitate requalification of the ET or any of its functions during launch. Thus the Shuttle has at present the capability to deploy in space a telescope whose size far exceeds its conventional payload capability.

The telescope essentially "down-converts" (in frequency) gamma-ray photons of energies greater than a few hundred MeV to pulses of a hundred optical photons of a few eV. This light is then focussed and detected using conventional methods. A large thin-walled, gas-tight, light-tight pressure vessel is essential for the technique to work. If the ET didn't exist, one would have to be designed in order to construct the telescope. A schematic of the

telescope after on-orbit assembly is shown in Figure 1.

The detection technique was originally conceived by Professor Kenneth Greisen (1966) of Cornell University. It has the virtues of

1. Simplicity of design
2. Extendibility to large areas
3. Inherently excellent immunity to non-gamma-ray background
4. Angular resolution approaching the theoretical limit.

In the early 1970's, Greisen's group in collaboration with SAO developed and flew a prototype several times on a high-altitude balloon (Albats, et al. 1971; Koch, et al., 1973), proving the concept. With it they were able to detect for the first time a discrete non-solar gamma-ray source of energy greater than 100 MeV (McBreen, et al., 1973). From additional flights, variability in the intensity and spectrum of gamma-rays from the Crab pulsar was also found for the first time (Greisen, et al., 1975). Subsequent measurements with COS-B have verified this phenomenon (Wills, et al., 1982).

By the time this mission would be carried out, a pointed telescope of this sensitivity would be required to study the sources catalogued by the forthcoming Gamma Ray Observatory (GRO). The GRO will be performing an all-sky survey.

In the process of developing the resources for this telescope many spinoffs will result that would have applications in areas related to the Space Station. These will include:

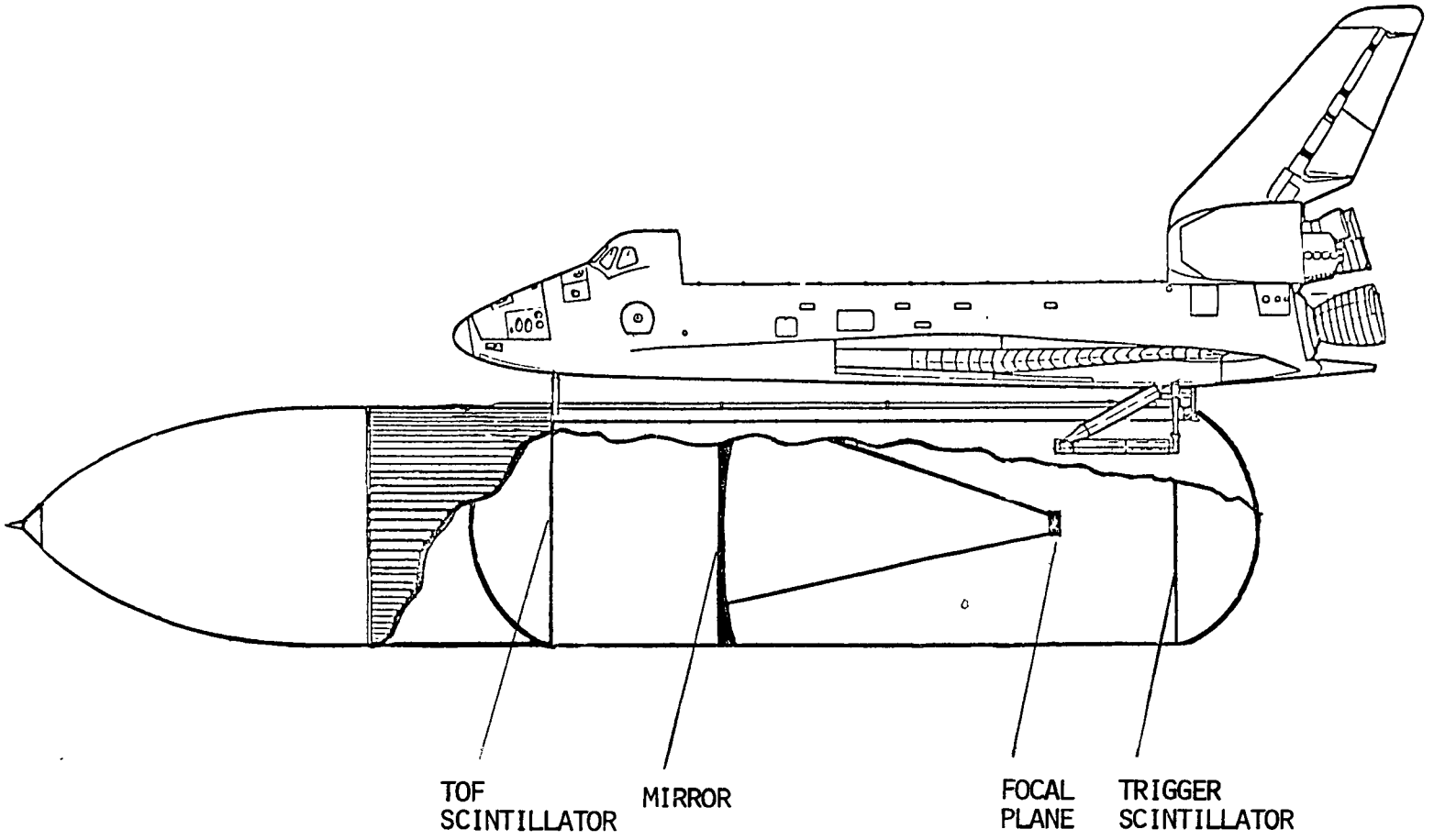

Figure 1. Gamma-ray imaging telescope system prior to separation. The support systems are not shown.

1. Demonstration that there are real applications for the ET on-orbit.
2. Attitude control, telemetry and power systems needed for this telescope could form the basis for using the ET as an unmanned platform.
3. The resealable manholes (possibly a docking adapter), gas pressurization system, meteoroid protection and thermal control along with point 2 could form the basis for using the ET as a manned platform.
4. Demonstration of the astronauts performing significant on-orbit assembly which is required for later more complex instruments such as the Large Deployable Reflector (LDR) and Space Station elements.
5. By packing, shipping, and performing final assembly on-orbit, it will be possible to deploy systems which otherwise could not be launched.
6. Pioneer a new era with less rugged components that would be packed rather than integrally strengthened to survive launch.

This report will summarize very briefly the field of high energy gamma-ray astronomy so that one can see that this telescope will meet the needs for the next phase of instrument development. A detailed description of the telescope will be given not only so one may understand how it works, but also so one can see that the ET is ideally suited for this application. The detailed description will also help to understand the reasons for the supporting requirements. A mission scenario is given a) to show that the nominal Shuttle

functions of delivering a payload to orbit will still be possible (i.e., the telescope would not significantly reduce the mission resources), and b) to identify the on-orbit activities. For convenience and to be able to provide specific detail, the scenario assumes the Orbiter as the work base. However, all the on-orbit activities could be carried out from the Space Station. Finally a synergetic approach to the mission could utilize and demonstrate many aspects of tethering, in particular

1. part of the attitude control system,
2. part of the energy storage for use on the night time of the orbit, and
3. part of the orbit reboost system.

Thus the capabilities developed for this telescope would form the basis for many of the components that would comprise a Space Station. Or vice versa, many of the components that would be needed for a Space Station could be utilized by this ET application.

2.0 EVOLUTION AND FUTURE GROWTH OF GAMMA-RAY ASTRONOMY

Gamma-ray astronomy is important for a complete astrophysical understanding of the Universe and how it functions, since gamma-rays are a direct measure of the presence and effects of energetic cosmic-rays. Charged primaries are absorbed and deflected as they propagate through space. However, the Galaxy and the Universe are essentially transparent to gamma-rays in the energy range of 10^7-10^{15} eV. There is only about a one-percent attenuation of the flux for a beam travelling through the galactic plane. Most importantly, their directional information is unchanged. Thus, gamma-ray observations directly provide spatial, spectral and temporal information about the source. High energy gamma-rays result directly or as secondaries from energetic processes, namely, electron-Bremsstrahlung, magneto-Bremsstrahlung (synchrotron radiation), inverse Compton scattering of star light and the microwave background, and by nuclear collisions. These processes take place in such diverse places as molecular and dark clouds, supernovae and pulsars, and in quasars and active galaxies. It is not the intent of this study to survey the field. Rather the reader is referred to a number of books on the subject (Greisen, 1971; Stecker, 1971; Chupp, 1976; and Fichtel and Trombka, 1981).

The predictions by Morrison (1958) and others lead to a flurry of optimistic attempts to detect gamma-rays with instruments flown on high altitude balloons. However, due to the very high flux of diffuse secondary gamma-rays produced in the residual atmosphere, it wasn't until the 1970's after many generations of detector development that the first unambiguous measurements were made using

very large detectors on the order of meters in area at altitudes in excess of 35 km or more. This has necessitated going to orbiting platforms.

The first significant results in high energy gamma-ray astronomy were those from OSO-3 (Kraushaar, et al., 1972). This detector consisted of scintillators and a Cherenkov counter. It had a sensitive area of 46 cm^2, a large field of view to permit surveying, and functioned for 16 months during 1967-1968. This instrument measured for the first time cosmic gamma-rays of energies above about 50 MeV. The celestial distribution consisted of a galactic plane component with an enhancement towards the galactic center and a diffuse extragalactic component. The next significant results came with the launching by NASA of the SAS-2 in November 1972 and by ESA of the COS-B in August 1975. These two detectors were very similar. Both were spark chambers with large fields of view for surveying and both were of about the same size, SAS-2 of 640 cm^2 and COS-B of 576 cm^2. The important difference being that COS-B operated for 81 months, versus SAS-2, which functioned for only 7 months. The results from these instruments showed that:

1. The galactic component had structure to it and can be correlated to the distribution of matter in the Galaxy,
2. The extragalactic component is diffuse and
3. 25 discrete sources have been identified. (See Bignami and Hermsen, 1983, for a review on gamma-ray sources.)

Of the 25 discrete sources, only four can be associated with known objects. These are the pulsars in the Crab and Vela nebulae (based

upon their pulsed radiation), the quasar 3C273, and the molecular cloud ρ Oph. (The latter two identifications are based solely on positional coincidences.) The remaining sources are unidentifiable primarily due to their positional uncertainty and possibly also because they may form a new category of astronomical object. Thus more sensitive detectors are necessary.

The detection process is hampered by two phenomena, reconstructing the direction of the primary gamma-ray and the very low fluxes. As an example, the strongest source above 100 MeV is the Vela pulsar with a flux of 10^{-5} photons/cm^2 sec., as compared to the strongest X-ray source in the 2-10 keV region Sco X-1, which has a flux that varies from about 20 to 40 photons/cm^2 sec. Hence, it is quite obvious that gamma-ray detectors must be orders of magnitude larger in collecting area to be able to detect sources with the same significance as in the X-ray region. The next step in progress is the GRO. This platform will be launched in the late 1980's aboard the Shuttle and contain another spark chamber, but of 6560 cm^2, ten times that of the previous two satellites. It too will be performing an all-sky survey. However, spark chambers are limited in their size by their complexity. Thus another form of gamma-ray detector of greater area is necessary to follow up the survey work. The need for such an instrument has been outlined in the "Field committee report" of the National Academy of Sciences - National Research Council (1982). Specifically (p. 165):

> "The Astronomy Survey Committee recommends the study and development of advanced gamma-ray experiments to follow the program to be carried out by the Gamma Ray Observatory (GRO).
>
> "Subsequent to GRO, an advanced high-energy

> gamma-ray telescope of very large area, high sensitivity, and high angular resolution will be needed for long-term observations of selected sources and regions of special interest. This will be necessary to achieve the statistical accuracy in the counting of gamma-ray photons required to resolve spatial and spectral features of the sources and to analyze their variations. The field of view of the telescope need not be wide, and an appropriate goal for angular resolution is the order of 1 to 2 arcmin."

The evolution of gamma-ray detectors has followed closely the evolution in launch capability. The instruments on GRO, although not straining the launch capability of the Shuttle, could not provide the necessary orders of magnitude increase in area within the conventional payload limits.

However, the telescope conceived of by Greisen would meet the recommendation set forth by the Astronomy Survey Committee and could be flown today with the existing Space Transportation System (STS), albeit in an unconventional fashion. Namely, this telescope would have a collecting area of $2.5 \times 10^5 cm^2$ and make use of the currently disposed-of ET by appropriately instrumenting it once on-orbit. THE ET IS IDEALLY SUITED FOR THIS SINCE A LARGE THIN-WALLED PRESSURE VESSEL IS NECESSARY AND IT IS AVAILABLE ON-ORBIT AT NO COST TO THE PAYLOAD CAPABILITY OF THE SHUTTLE OR THE SCIENCE BUDGET OF NASA. The prototype of this telescope has been proven to be an astrophysically useful tool, and with the culmination of the Shuttle and its ET, the GRO survey, and the starting of the Space Station, the time for deployment of this telescope has come. The results of this concept definition show how this can come about.

3.0 TELESCOPE -- TECHNICAL DISCUSSION

3.1 Detection Technique

The best way to describe how the telescope works is to trace the sequence of events necessary to identify a gamma-ray event. Presume a high energy gamma-ray is incident onto the detector roughly parallel to the telescope axis; refer to Figure 2 for notation. Since the container walls are relatively thin, the probability of being converted in passing through the aft LH_2 tank dome is small. The first element used to mark the signature is the veto scintillator, S1. A sheet of plastic scintillator will produce a very fast pulse of light caused by the ionization of charged particles passing through it. S1 is used to reject all charged particles. The gamma-ray, being neutral, will not be detected by S1 and the probability of its being converted is also small. Next the gamma-ray enters the converter, nominally lead. Since the converter is a small fraction of a radiation length thick, say .036, the probability of the gamma-ray being converted into an electron-positron pair is .028. Although the pair will emerge from the converter with a total energy nearly equal to that of the incident gamma-ray, the emission angle of the secondaries and multiple Coulomb scattering within the converter will cause each particle in the pair to deviate somewhat from the incident gamma-ray direction. The pair immediately enters the second scintillator, S2. This time a pulse is produced, and in fact the pulse amplitude will be indicative of a two-particle event. Next the pair travels the length of the telescope, emitting Cherenkov light as it passes through the gas (see the next section for a discussion of Cherenkov

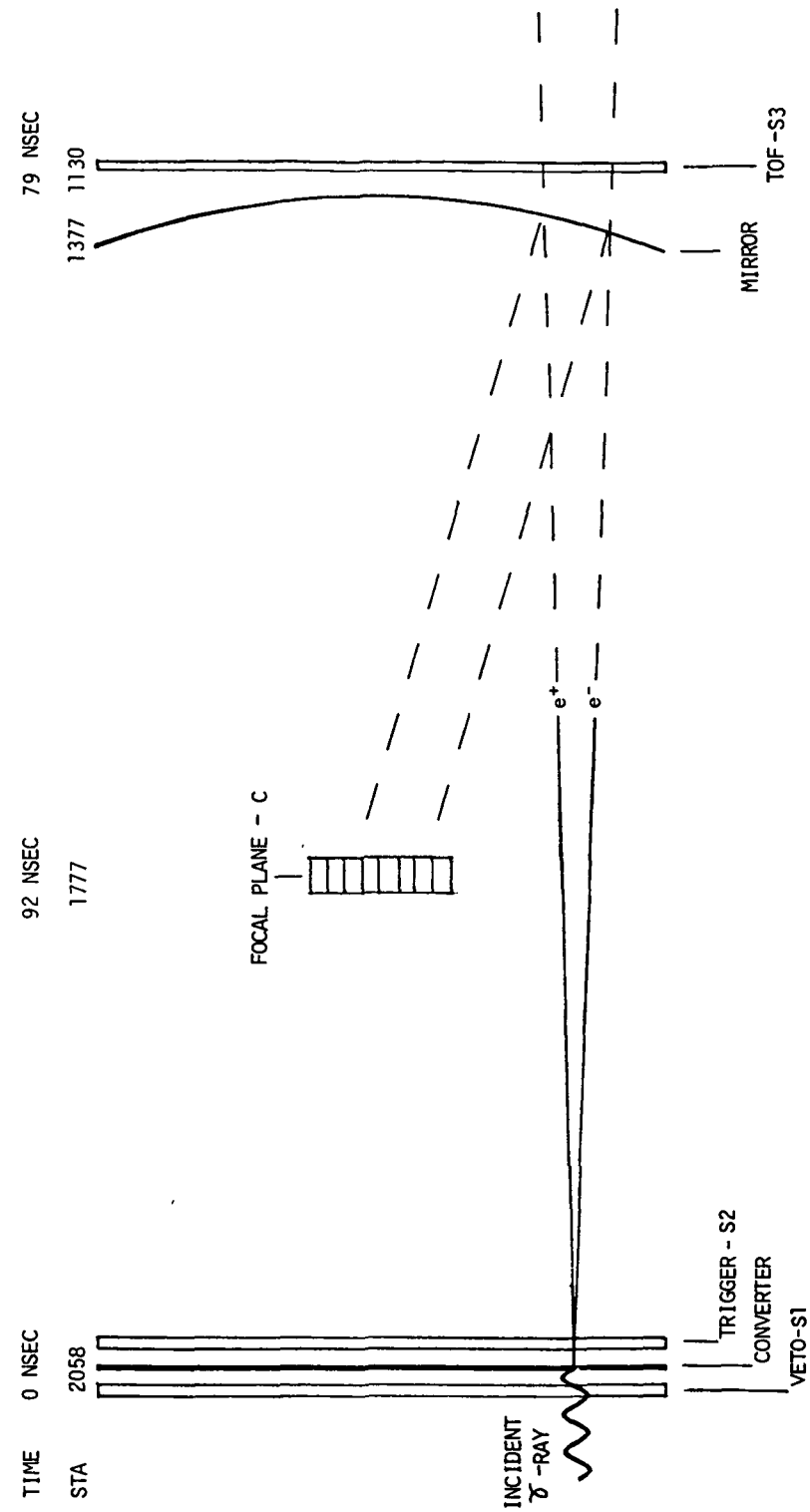

Figure 2. Schematic to show concept. Not to scale.

radiation). This light is then imaged by the optical system onto an array of photomultipliers in the focal plane, C (see Figure 3). Pulse height analysis of the array will enable reconstruction of the two rings of light and thus determine the incident gamma-ray direction. After the pair continues through the mirror it passes through a third scintillator, S3. This third scintillator is incorporated to provide an additional time of flight, TOF, measurement and reduce the chance coincident rate, particularly from backwards-going particles. Thus the electrical signal that will uniquely identify a gamma-ray event will be $\overline{S1(t)} * S2(t) * S3(t+79) * C(t+92)$; that is, a pair triggers S2 with no simultaneous veto signal in S1; 79 nsec later (1 nsec = 10^{-9} sec) the pair is detected in S3, and 92 nsec after pair creation takes place in the converter the light indicative of two Cherenkov rings arrives at the focal plane.

The salient features of this detection technique are that:

1. The active collecting area can easily be made very large to detect the very low fluxes without significantly increasing the complexity of the instrument.
2. The telescope has excellent background rejection properties. This is discussed in great detail in a later section but in summary:
    a. The veto, converter and trigger form a tightly packed sandwich.
    b. The large component spacing and threefold time-delayed coincidence eliminates backwards-going events and reduces random processes to a negligible rate.

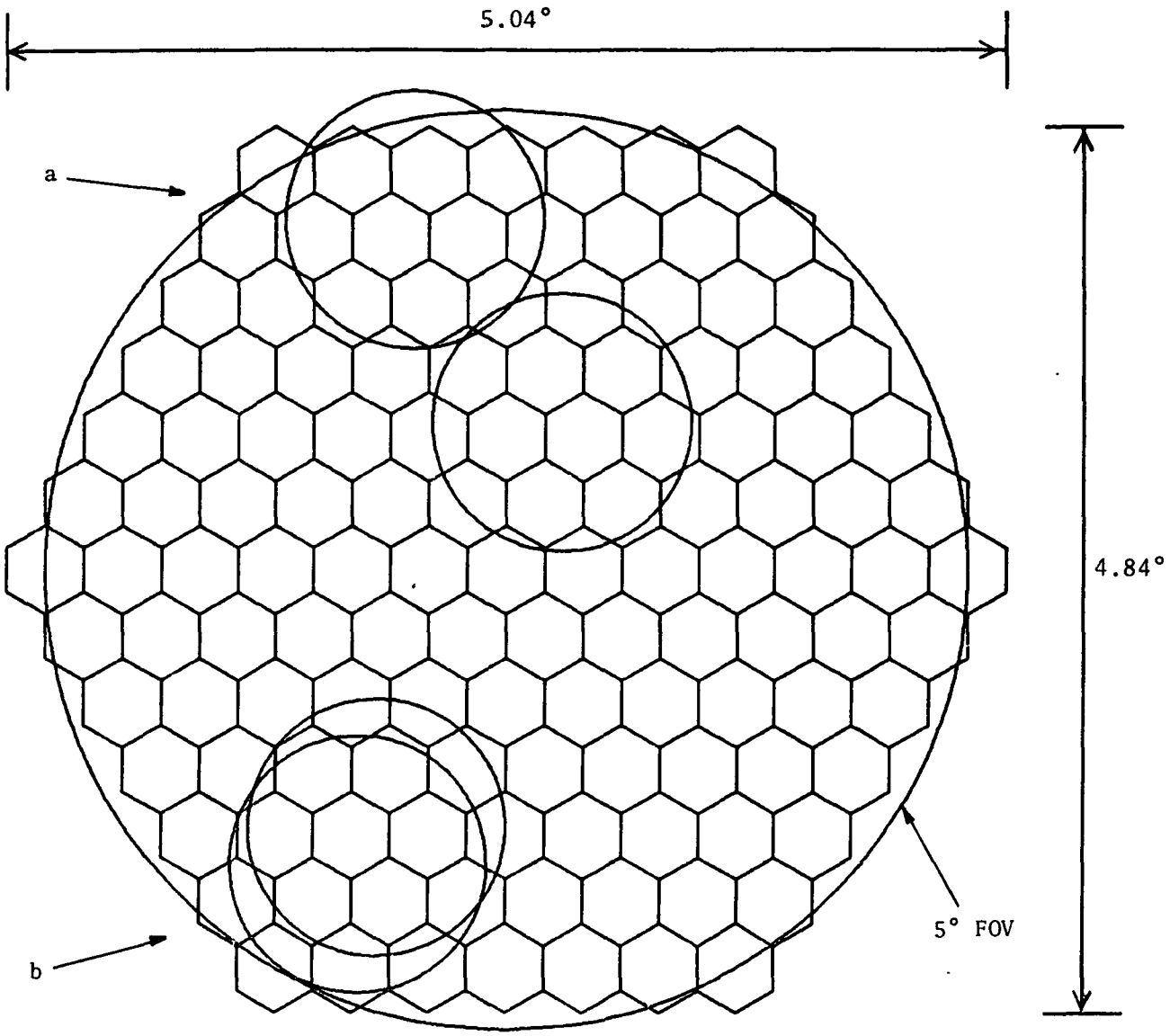

Figure 3. Layout of the focal-plane array. The focal plane consists of 127 resolution elements. Each cell contains a phototube and light pipe. A pair of rings are shown for a) a typical low-energy event and b) a typical high-energy event. The cone diameters are 1.4° and the center-to-center cell spacing is 0.42°.

c. The Cherenkov process requires particles of a large Lorentz factor [see equation (1) of the next section].

d. The mirror images the light into two unique well defined rings of light.

3. Since very fast (nanosecond) logic signals are used throughout, the instrument is virtually deadtimeless. And although gamma-ray bursts have not yet been detected at several hundred MeV, this instrument is capable of detecting bursts of very high fluxes without being jammed.

3.2 Properties of Cherenkov Radiation

The character of the Cherenkov process is as follows: whenever a charged particle passes through a media with a velocity greater than the velocity of light in that media, it will emit light. The threshold velocity, the angle of emission Θ and the number of photons emitted ξ are all related to the index of refraction, n.

Briefly summarized here are a number of properties of the Cherenkov radiation process. For highly relativistic particles, the relationship between the energy, E, velocity, v, and Lorentz factor γ is given by:

$$E = m_o c^2/(1-v^2/c^2)^{1/2} = \gamma m_o c^2 \qquad (1)$$

where m_o is the particle rest mass and c is the velocity of light in a vacuum. In a dielectric medium the velocity of light is less than c, specifically

$$v = c/n \tag{2}$$

where n is the index of refraction. Whenever a charged particle passes through a medium with a velocity greater than the velocity of light in a media, that is, the charge moves faster than its associated field can propagate, it will emit Cherenkov light quite analogous to a bow wave or sonic boom. Combining (1) and (2) gives the threshold Lorentz factor γ_T.

$$\gamma_T = 1/(1-1/n^2)^{1/2} \simeq 1/(2\eta)^{1/2} \tag{3}$$

where $\eta = n - 1$ provided $\eta << 1$. Figure 4 shows this relationship.

The geometry of the phenomena, that is, the angle of the coherent wave front, dictates that the radiation is emitted at a specific angle, θ, from the direction of propagation given by:

$$\cos\theta = c/nv \ . \tag{4}$$

At threshold $c = nv$ and $\theta = 0$. When $v = c$, $\cos\theta = 1/n$ which is the maximum angle of emission. Combining this with (3) and using the small angle approximation for cosines gives

$$\theta_c = 1/\gamma_T \ . \tag{5}$$

Combining (1) and (4) and assuming $\gamma >> 1$ yields the relationship for the emission cone half angle as a function of the Lorentz factor γ.

$$\theta^2/\theta_c^2 = 1 - \gamma_T^2/\gamma^2 \ . \tag{6}$$

This is shown in Figure 5. It can be seen that the cone angle rises very rapidly to near its asymptotic value.

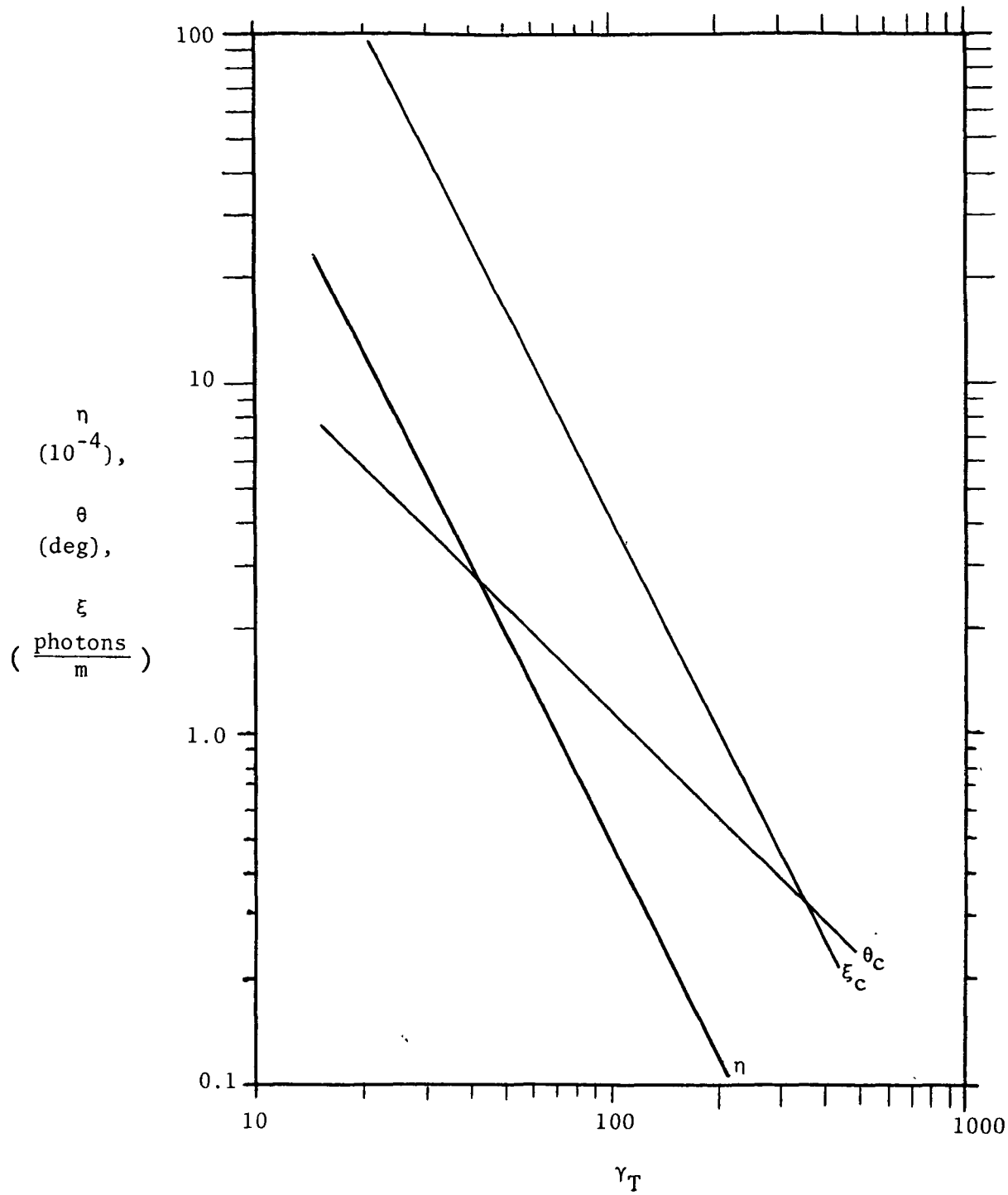

Figure 4. Cherenkov parameter dependence on the threshold Lorentz factor. $\eta = n-1$ (n = index of refraction), cone angle, θ_c, and light production, ξ_c, vs. the selected threshold Lorentz factor, γ_T.

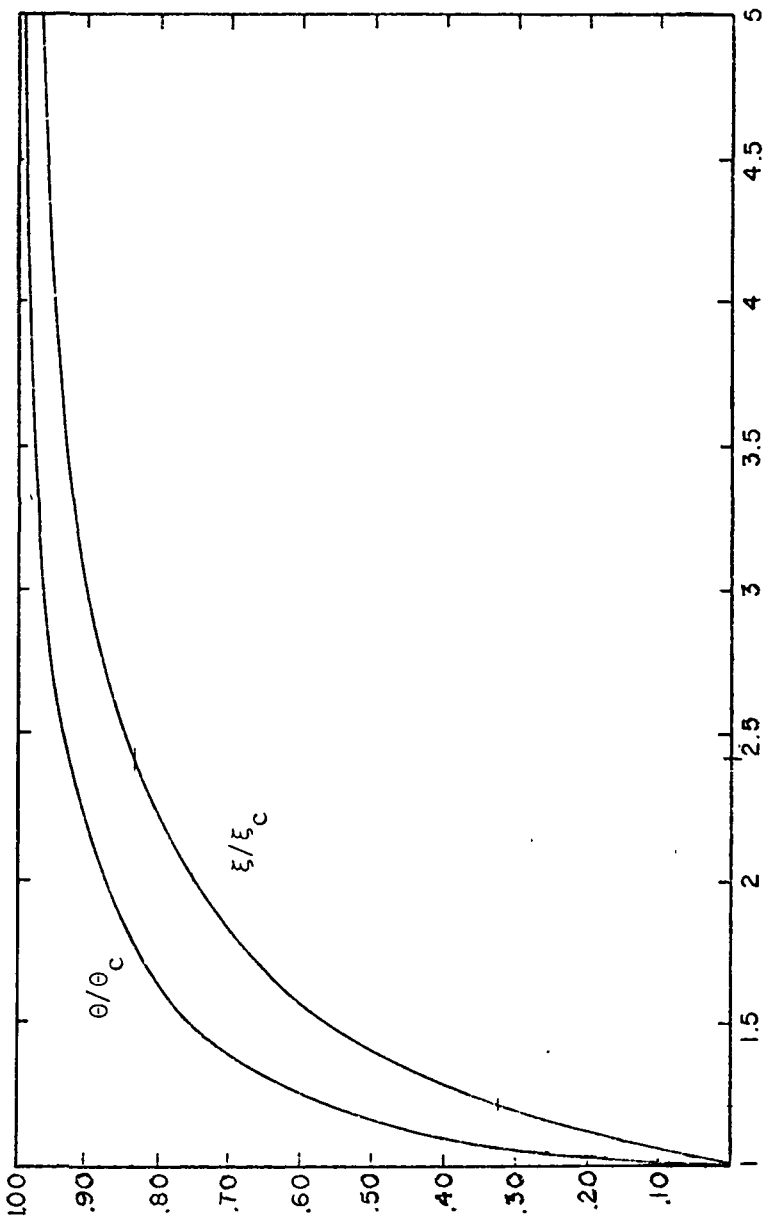

Figure 5. The relative Cherenkov radiation ratio ξ/ξ_c and relative cone diameter θ/θ_c vs. energy relative to threshold.

The final quantity that depends on the threshold Lorentz factor is the amount of light emitted per unit path length, ξ. The energy radiated in the near UV through visible is given by

$$\xi = 400 \sin^2 \theta \text{ photons/m} . \quad (7)$$

At threshold $\sin\theta = 0$ and $\xi = 0$. As the particle approaches the velocity c,

$$\xi_c = 400 \sin^2 \theta_c = 400/\gamma_T^2 . \quad (8)$$

This is also shown in Figure 4. For intermediate velocities, the above equations can be combined to yield the relationship of light production as a function of Lorentz factor:

$$\xi/\xi_c = 1-\gamma_T^2/\gamma^2 . \quad (9)$$

This is also shown in Figure 5.

3.3 Sensitivity

The primary features by which nearly all astronomical instruments are measured are sensitivity, angular resolution, and energy resolution. Fortunately, in this portion of the spectrum a general criterion can be derived in a rather straightforward manner with little or no approximating. The sensitivity or statistical significance in terms of the number of sigmas above the background, NSIG, for Gaussian statistics is the source strength (after background subtraction) divided by the standard deviation of the background. This is given by

$$NSIG = N_S/N_B^{1/2} \tag{10}$$

where N_S is the number of counts from the source and N_B the average counts due to the sum of all sources of background. The source counts are given by

$$N_S = \alpha\ \delta\ I_S\ A\ t\ d\ \varepsilon_c \tag{11}$$

where

$\alpha = \exp(-7r_A/9)$ = attenuation of the incident gamma-ray flux due to the overlying materials, r_A in radiation lengths.
α is close to unity since the average thickness of aluminum overlying the detector is a small fraction of a radiation length.

δ = fraction of counts within resolution element, Ω, = .632.

I_S = source flux above the threshold in photons/cm^2/sec.

A = sensitive area in cm^2.

t = exposure time in seconds.

$\varepsilon_c = [1 - \exp(-7r/9)]$ = conversion efficiency, r in radiation lengths for Bremsstrahlung. For the energies of interest, the asymptotic limit is used.

d = duty cycle equal to one minus the fractional dead time and is essentially unity for this detector.

The background counts are given by

$$N_B = \alpha\ I_D\ A\ t\ d\ \varepsilon_c\ \Omega + \Sigma N_{Bi} \tag{12}$$

where

I_D = diffuse gamma-ray background flux above the threshold in photons/cm^2/sec/sr

$\Omega = \pi\Sigma\theta_i^2$ = solid angle of resolution element due to various random effects.

N_{B_i} are those portions of the non-gamma-ray backgrounds which cannot be rejected. Ω is taken to be the solid angle within which different directions can not be distinguished and within which the possibility for detection of an event from a point source is high. θ is the result of a random process (emission angle and multiple Coulomb scattering). For a two-dimensional random walk process, the probability of emerging with an angle less than θ is

$$P(<\theta) = 1 - \exp(-\pi\theta^2/\Omega) \qquad (13)$$

($\theta \lesssim 2^o$, Bethe, 1953).

The effects that contribute to the resolution element are the following:

1. Emission angle of the secondaries.

$$\theta_e^2 = [q' \ (.51 \text{ MeV/E}) * \ln (E/.51 \text{ MeV})]^2$$

$$= (21 \text{ MeV/E})^2 * [.0243 \ln (E/.51)]^2 \qquad (14)$$

where q' is a slowly varying function of order unity and E is the primary energy in MeV.

2. Secondary scattering in the lead converter as a result of multiple Coulomb scattering.

$$\theta^2_{Pb} = [21\ MeV/(E/2)]^2 * r * (4/9)$$

$$= (21\ MeV/E)^2 * 16r/9 \qquad (15)$$

where the secondary energy is taken to be about E/2 and r is the converter thickness in radiation lengths. The 4/9 results from the secondary scattering only after its creation; i.e., the average scattering is only 2/3 the value it would be for a particle always traversing the entire thickness.

3. Secondary scattering in the trigger scintillator.

$$\theta^2_S = [21\ MeV/(E/2)]^2 * (.4/42.4)$$

$$= (21\ MeV/E)^2 * .0377 \qquad (16)$$

where 4 mm thick plastic scintillator is assumed. A radiation length in plastic scintillator of 42.4 cm.

4. Scattering in the gas while radiating.

$$\theta^2_R = [21\ MeV/(E/2)]^2 * (1730/1.26 \times 10^5) * (4/9)$$

$$= (21\ MeV/E)^2 * .02448 \qquad (17)$$

where N_2 gas is assumed, a radiation length at 3.56 psi is 1.26×10^5 cm and the 4/9 results from the average scattering in the gas since once the Cherenkov photon is emitted its direction is unaffected by further scattering of the secondary.

5. Measurement error in reconstructing the direction of each secondary θ_m.

In Section 3.8 it will be argued that the non-gamma-ray backgrounds are insignificant; therefore, the signal to noise can be written as

$$NSIG = N_S/N_B^{1/2} = \delta I_S (\alpha A t d \varepsilon_c/I_D\Omega)^{1/2}$$

$$= \delta I_S (\alpha A t d/\pi I_D)^{1/2} * h(r,E) * (E/21 MeV) \quad (18)$$

where

$$h^2(r/E) = [1-\exp(-7r/9)] /$$

$$\{[.0243 \ln (E/.51)]^2 + 16r/9 + .0622 + (\theta_m E/21)^2\} \quad (19)$$

The function h contains the instrument dependence on energy, converter thickness, and measurement error. This function is shown in Figure 6. When $\theta_m \lesssim 5$ arcmin, the quantity h(r,E) depends very slowly on E and for the energies of interest (200 MeV to 2 GeV) the denominator can be approximated as 16r/9 + 0.09. Then for the asymptotic cases,

$h(r,E) \simeq 2.93\ r^{1/2}$ $(r << .01)$ and

$h(r,E) \simeq .75\ r^{-1/2}$ $(r >> 1)$.

The peak in h(r,E) = .58 occurs near 1/3 radiation length and remains within 10% of the peak for $0.09 \lesssim r \lesssim 1.2$. Even at $.036 < r < 2.7$, h(r,E) is within 75% of its peak. Hence for a wide range of values of r, $h \simeq 0.5$ if $\theta_m \lesssim 5$ arcmin and then

$$NSIG \simeq I_S(\alpha A t d/I_D)^{1/2} * E/117 . \quad (20)$$

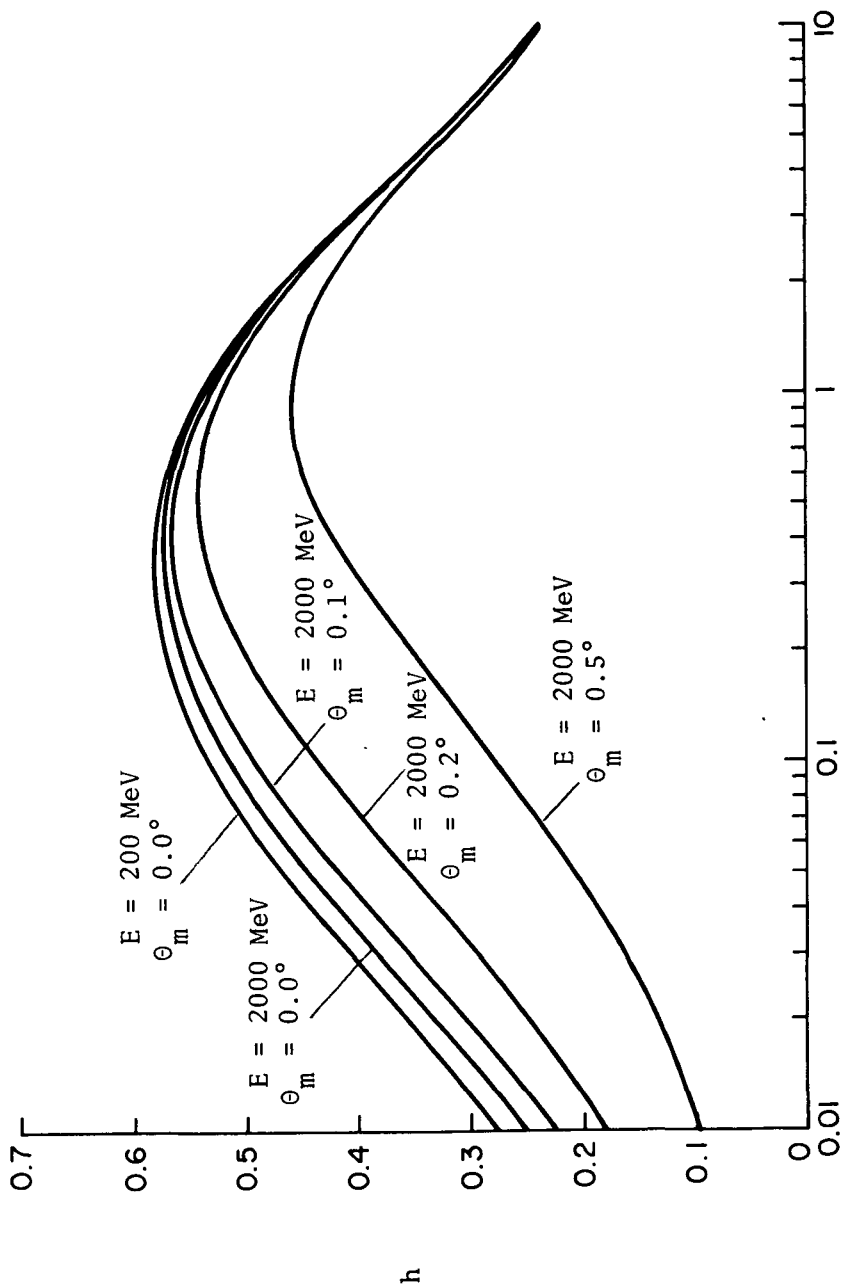

Figure 6. Instrument detection efficiency vs. converter thickness. The function h contains the instrument dependence on energy, converter thickness, and measurement error, Θ_m. For $E \lesssim 200$ MeV, h is nearly independent of Θ_m.

When the measurement error θ_m is not negligible NSIG is reduced at the higher energies. This is shown in Figure 6 by curves for θ_m = 0.1, 0.2, and 0.5°. For this telescope θ_m should be less than or on the order of 0.1°. IT IS VERY IMPORTANT TO NOTE THAT THE STATISTICAL SIGNIFICANCE DEPENDS ALMOST ENTIRELY ON THE COLLECTING AREA AND LIVE TIME; AND IT IS ESSENTIALLY INDEPENDENT AT THESE ENERGIES OF ALL OTHER INSTRUMENTATION PARAMETERS PROVIDED THE MEASUREMENT ERROR IS KEPT SMALL. Therefore, to first order the larger the area, the greater the sensitivity.

The NSIG given by (20) has been considered so far in terms of the instrumental effects, but it also depends on the spectrum of the source and background, in particular I_S and I_D, which are the integral fluxes above a given energy. The results from COS-B (Bignami and Hermsen, 1983) indicate that a typical source spectral dependence is of the form $dN/dE \propto E^{-2}$; that is, $I_S \propto 1/E$. The galactic background dependence given by Hartman, et al. (1979) is $dN/dE \propto E^{-1.7}$, that is $I_D \propto E^{-0.7}$. Inserting these dependences into (20) gives

$$NSIG \propto E^{0.35} . \qquad (21)$$

IT IS RATHER AMAZING THAT NSIG INCREASES WITH ENERGY EVEN THOUGH THE DIFFERENTIAL SPECTRAL INDEX IS DROPPING OFF ALMOST THREE TIMES AS FAST AS THE BACKGROUND. (This is true up to an energy where the source intensity is cut off.) Not only is NSIG better at the higher energies, but also the angular resolution is better, as will be shown in the next section. Thus to make significant progress in gamma-ray astronomy it is important to work at the higher energies.

And to do this will require a large-area detector such as this one.

3.4 Angular Resolution

The angular resolution has different meanings in different contexts; in particular, it may refer to the minimum separation necessary to distinguish two point sources or to map an extended region of emission, or it may refer to the positional uncertainty of the centroid of events for an isolated point source.

3.4.1 Peak-to-Peak Angular Resolution

The peak-to-peak angular resolution will be taken to be a quantity analogous to what is commonly referred to as the full width at half maximum. As described in the previous section, various random processes cause the incident gamma-ray beam to produce a two-dimensional distribution of events about the incoming direction, (13). The resolving power for peak-to-peak separation, θ_{pp}, will be defined to be the angle within which $1 - 1/e = 63.2\%$ of the events are distributed. That is, θ_{pp} will be taken to be twice the rms angle for the gamma-ray direction. The rms angles given in the previous section were for one of the electrons in terms of the primary gamma-ray energy. Combining the directions from a pair reduces the rms uncertainty by $\sqrt{2}$. Therefore

$$\theta_{pp} = \sqrt{2}\,(\theta_e^2 + \theta_{Pb}^2 + \theta_S^2 + \theta_R^2 + \theta_m^2)^{1/2} . \qquad (22)$$

One of the major objectives of this telescope is to improve on the angular position; that is, to have θ_{pp} as small as possible. First of all the ultimate resolution is limited by the emission angle θ_e

of the pair when they are produced. Secondly, as shown in the previous section, the statistical significance is independent of the converter thickness for a wide range of thickness, provided the converter is thicker than the scintillator in radiation lengths. Therefore it is important to use a converter thickness that will minimize the scattering without severely reducing NSIG. A converter thickness of r = 0.036 radiation lengths seems to be a reasonable tradeoff between angular resolution and a small reduction in NSIG. The scintillator thickness has been minimized to what is probably the thinnest practical. The calculations assumed N_2 as the gas. However, if H_2 were used, the radiation length of the gas could be reduced by a factor of ten. Table 1 gives the peak-to-peak resolution for a number of primary energies. IN SUMMARY, THE PEAK-TO-PEAK ANGULAR RESOLUTION IS WITHIN A FACTOR OF TWO OF THE ULTIMATE ACHIEVABLE DUE TO THE EMISSION ANGLE AND COULD POSSIBLY BE IMPROVED BY USING H_2. Also note that the resolution is nearly inversely proportional to the energy. It is recommended that a scintillator module be constructed to determine the minimum thickness of scintillator that can be used. It is also recommended that the necessary tradeoffs between the various possible gases be conducted as soon as possible.

Table 1

Peak-to-Peak Angular Resolution Vs. Energy

Process	Thickness in Radiation Lengths	Θ_{rms} for Given Incident Gamma-Ray Energy 250 MeV	500 MeV	1 GeV	2 GeV
Emission Angle	NA	0.72	0.40	0.22	0.12
Coulomb Scattering					
Converter	0.036	1.22	0.61	0.30	0.15
Scintillator (4 mm)	0.00943	0.93	0.47	0.23	0.12
Gas (N_2)	0.00612	0.75	0.38	0.19	0.09
Θ_m	NA	0.10	0.10	0.10	0.10
$\Theta_{rss} = (\Sigma \Theta_i^2)^{1/2}$ (per particle)	NA	1.86	0.95	0.49	0.27
Θ_{rss} (per event)	NA	1.32	0.67	0.35	0.19
$\Theta_{pp} = \sqrt{2}\Theta_{rss}$	NA	2.63	1.34	0.70	0.37

Note that all angles are in degrees.

The fact that two secondaries are produced for each primary, to first order, will not affect the shape of the distribution. The division of energy between the electron and positron is in general not equal. In this case the particle of lower energy will scatter more. Because the ring of light will also be blurred due to the Coulomb scattering in the gas and since it produces measurably less Cherenkov light, it can be discriminated against in favor of the higher energy particle having less scattering. The net result is that the peak-to-peak resolution should be slightly better than what is derived here.

3.4.2 Centroid Uncertainty

Although a number of random processes cause a collimated beam of gamma-rays to produce an extended peak about the incident direction, in the limiting case of infinite statistical significance and infinitesimally small resolution elements, the centroid of the distribution could be located with absolute precision. However, as in all cases, the size of the resolution element and NSIG are finite. In what follows it will be assumed that NSIG will be large enough so that the positional uncertainty is dominated by the size of the resolution element.

In the simplest case, for a rectangular distribution with a yes/no criterion in each cell, the positional uncertainty is simply one-half the cell size. The situation improves by 1/N where N is the number of gradations within each cell. Because of the unusual geometry of rings of light, the hexagonal cell shape, and the small number of photoelectrons defining each ring (an average of three per cell) an analytic expression for the uncertainty of the centroid's position can not easily be derived. It is recommended that a Monte Carlo simulation be performed for an ET configuration using the Chi-squared method to determine the uncertainty.

In the configuration as proposed the center-to-center angular distance of each cell is 0.42 degrees. Assuming that the uncertainty is at least as good as in the simplest case and probably is on the order of three times better (due to the average of three photoelectrons per cell), the positional uncertainty for the limiting case of very large NSIG is on the order of 0.07 to 0.21 degrees or 4 to 13 arcminutes for an isolated point source.

3.5 Anticipated Count Rates

In order to appreciate the sensitivity of this telescope it is useful to see what the count rates will be from already known sources and compare them with the previous detectors. The two pulsars will be considered. First of all the background flux from the Galaxy in the region around these sources is about

$$I_D = 0.3 \times 10^{-4} \text{ photons/cm}^2 \text{ sec sr } (E > 300 \text{ MeV})$$

(Mayer-Hasselwander, et al., 1982). From (12) the background rate is

$$R_B = \alpha I_D A \varepsilon_c \Omega . \tag{23}$$

For the ET, the aft dome wall thickness is on the order of .034 radiation lengths so that $\alpha = .97$. The active area will be taken as $2.4 \times 10^5 \text{cm}^2$. The conversion efficiency will be taken to be .0276 (.036 radiation lengths) and a resolution element to be $\Omega = 1.15 \times 10^{-3}$ sr ($\theta = 1.1$ at 300 MeV from Table 1). Then

$$R_B = 7.26 \, I_D \text{ counts/sec/resolution element}$$
$$= 0.8 \text{ counts/hr/resolution element } (E > 300 \text{ MeV})$$

The maximum counting rate occurs around the galactic center where $I_{GC} = 2 \times 10^{-3}$ photons/cm^2 sec sr ($E > 200$ MeV), $\Omega = .006$ sr ($\theta = 2.5$) for the field of view. Then $R_{GC} = 1.2$ cnts/min ($E > 200$ MeV). Using the intensities and spectral parameters from Bignami and Hermsen (1983), the intensities for the Vela and Crab pulsars ($E > 300$ MeV) are respectively

$$4.75 \times 10^{-6} \text{ and } 0.67 \times 10^{-6} \text{ photons/cm}^2 \text{ sec}.$$

From (11) the source rate is

$$R_S = \alpha \delta I_S A \varepsilon_c = 4060 * I_S \text{ counts/sec} . \quad (24)$$

Thus the Vela and Crab rates are

R_V = 70 counts/hr and

R_c = 9.8 counts/hr

or in one hour the number of sigma above background will be

$NSIG_V$ = 78 and $NSIG_c$ = 11.

As a comparison, in a combination of five observations of the Crab, totaling 189 days with the COS-B (Wills, et al., 1982), 1733 gamma-rays were detected from the region of the Crab. Of these, about 1265 were background, leaving a signal of 468 or a NSIG = 13.2. In addition to a comparison of the statistical significance the comparison of signal to noise can be made. For the Crab measurement by COS-B, the measured value of 1733 has an uncertainty of 41.6. Assuming that the background uncertainty is small compared to this, then the signal to noise is (1733 - 1265)/41.6 = 11.2. For this telescope, the signal will be 9.8t and the noise will be $[(9.8 + 0.8) \times t]^{1/2}$. The signal to noise will reach 11.2 in 13.8 hours; that is, a light curve with the equivalent signal to noise of that given by Wills, et al., requiring half a year of integration could be obtained with this telescope in just over half a day of integration. This points out the fact that the increase in area of this telescope relative to COS-B of about 420 is roughly equal to the reduction in integration time of 330 for this telescope to obtain a comparable signal to noise. Thus, one can see how much more sensitive this telescope is

compared to the previous satellites. The sensitivity of GRO will be somewhere between that of COS-B and this telescope. THIS GREATER SENSITIVITY WILL PERMIT MEASUREMENT OF SHORT-TERM TEMPORAL PHENOMENA WHICH WOULD OTHERWISE NOT BE POSSIBLE WITH A SMALLER DETECTOR.

3.6 Energy Resolution

In addition to determining the arrival time and direction of each gamma-ray it is useful to know its energy. For it is from the spectral distribution of photons that the source mechanism is generally understood. In the radio and infrared portions of the spectrum one sees molecular transitions, in the visible and X-ray one sees atomic transitions, and in the gamma-ray there are the nuclear transitions and interactions. In addition there are continuum spectra both thermal and non-thermal. The bulk of the nuclear lines are in the energy range of 1 to 10 MeV (see Chupp, 1976). The only distinctive gamma-ray spectrum at higher energies is due to pion decay. The decay spectrum from isotropically moving π^o mesons has a maximum at $E_m = m_\pi c^2/2 = 68$ MeV. Pions of energy $\gamma m_\pi c^2$ produce a flat decay spectrum from $E_m/2\gamma$ to $2\gamma E_m$. The the gamma-ray spectrum from a non-mono-energetic source will have a very broad distribution peaked at 68 MeV. THUS IN THE HIGH ENERGY REGION (E > 100 MeV) THERE IS LITTLE NEED FOR FINE ENERGY RESOLUTION SINCE ALL THERE IS TO MEASURE ARE CURVATURES, SLOPES, AND CUTOFFS OF CONTINUUM SPECTRA. Therefore in this telescope there is no major effort to obtain fine energy resolution.

The inherent energy resolution for a single event is obtained from a measurement of the separation of the electron-positron pair due to their emission angle and multiple Coulomb scattering. The differential probability distribution for the opening angle is

$$dP/d\theta = (\theta/\theta_p^2)\ \exp(-\theta^2/2\theta_p^2) \qquad (25)$$

where $\theta_p^2 = \theta_{rms}^2/2$ is the most probable opening angle. The probability that the measured opening angle θ_m results from a gamma-ray at an energy E which is different from the most probable energy E_m is

$$dP/d\theta = (\theta_m/\theta_p^2)\ \exp(-\theta_m^2/2\theta_p^2) \qquad (26)$$

where θ_p is the peak probability for energy E. The peak probability is $(\theta = \theta_p)$

$$dP/d\theta = (1/\theta_p)\ \exp(-1/2)\ . \qquad (27)$$

Dividing (26) by (27) gives the normalized likelihood for getting θ_m when θ_p is expected. From Table 1 it is clear that the rms scattering and hence the rms opening angles are nearly inversely proportional to E. Thus

$$E/E_m \simeq \theta_m/\theta_p\ . \qquad (28)$$

Substituting this into the ratio of (26) and (27) gives

$$\mathcal{L} = E/E_m * \exp(1/2 - E^2/2E_m^2)\ . \qquad (29)$$

This function is plotted in Figure 7. The likelihood ratio is 0.5 for $E/E_m = 0.32$ and 1.92. This defines the energy resolution for a single event. Combining the measured energy distribution with the

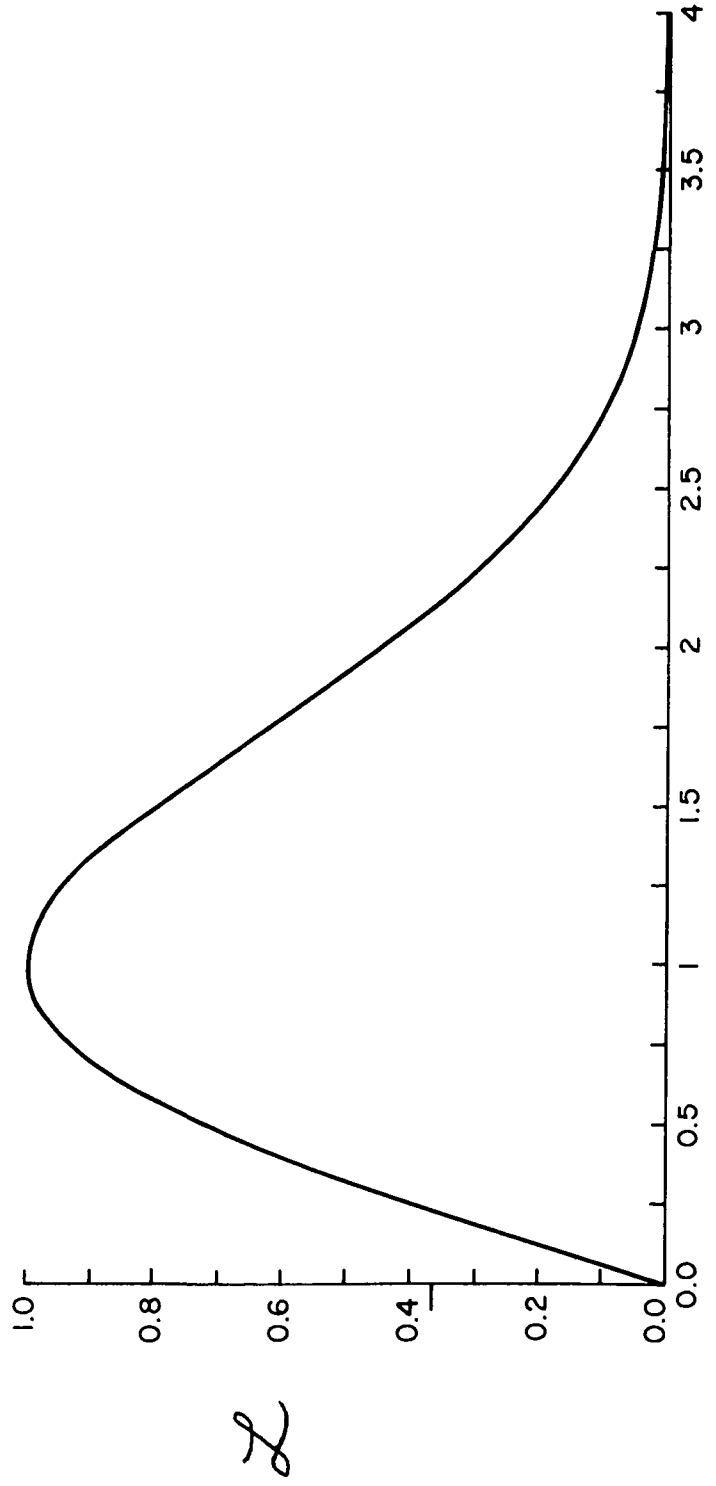

Figure 7. Single event energy uncertainty. The normalized likelihood for a gamma-ray event having been assigned an energy E_m, really being due to a gamma-ray of a different energy E.

known instrument performance, it will be possible to perform least squares fits to determine source spectra.

Improved energy resolution at these high energies could be accomplished if desired in a number of ways.

1. A total absorption calorimeter as has been used with the smaller spark chambers. This unfortunately would be very heavy, requiring at least ten radiation lengths of material. Also, the cost of the traditional NaI or CsI crystals would be truly astronomical.
2. A somewhat lighter and quite practical system would be a shower counter composed of layers of scintillators and lead. But even one radiation length of lead (6.37 gm/cm^2), which would be a barely useful thickness, placed behind the mirror (area $\simeq$ 5 x 10^5 cm^2) would weigh 3185 kg (7030 lbs.). However, this should not be ruled out as a future possibility.
3. Transition radiation detectors (Swordy, et al., 1982) have been investigated. They are quite attractive for measuring the higher energies E > 500 MeV since they do not require total absorption of the particle energy and are relatively lightweight. However, since the active components are gas-filled proportional counters, the necessary equipment would more than exceed in complexity the rest of the telescope.

3.7 Threshold Selection and Radiating Gas

There are many factors that influence the selection of the energy threshold for this telescope. The threshold for generating Cherenkov light is determined by the Lorentz factor $\gamma = E/mc^2$ where E is the energy and m the rest mass of the particle.

In order to be immune to the decay products of muons (maximum energy 53 MeV) that could stop and then decay in the converter, the threshold, γ_T, should be 100. This eliminates the need for a long veto pulse of 10 microseconds. Another reason for setting γ_T high is to ensure that the gamma-rays interact purely by the pair production mechanism. At 20 MeV (in aluminum) the Compton scattering and pair production cross sections are about equal. At 100 MeV the pair production cross section is ten times the Compton and also has nearly reached its asymptotic value. Finally, the multiple Coulomb scattering is worse at lower energies and as shown in Section 3.3 the statistical significance as well as the angular resolution actually decrease with decreasing energy.

The argument for keeping γ_T as small as possible is that the light production goes inversely as the square of γ_T [equation (8)]. Thus there is no hard and fast rule for quantitatively determining γ_T. A value of $\gamma_T = 83$ had been used in the previous generation of this telescope and for a lack of a good reason for change, this value will be used here. From (3) the index of refraction corresponding to $\gamma_T = 83$ is $n = 1.0000726$ ($\eta = 72.6 \times 10^{-6}$). The asymptotic ring diameter is 1.38 degrees and the asymptotic number of photons produced per particle is 5.8 per meter. If a selection criterion is set to require detection of at least 80%of the light in

each ring, then from (9) the effective threshold will be $\gamma_{eff} = 186$. ASSUMING EQUAL DIVISION OF THE ENERGY BETWEEN THE PAIR, THE EFFECTIVE THRESHOLD FOR GAMMA-RAY DETECTION WILL BE ABOUT 182 MeV.

None of the above constraints dictates the particular gas, but only defines the index of refraction that is the gas density. Figure 8 shows the pressure vs. Cherenkov threshold for various gases. (Others may also be considered along with gas mixtures.) For $\gamma_T = 83$ the pressures would be 7.62, 3.56, 4.01, and 2.60 psia for H_2, N_2, O_2, and CO_2 respectively. These values are all safely within the ET operating pressure limit of 40 psi. From this list, the preferred gas would be H_2 simply because the thickness of the gas in radiation lengths is less than one-tenth that of any other gas for this index of refraction. This would reduce the scattering in the gas to a negligible level. Two other reasons H_2 comes to mind is that the vessel being used is the LH_2 tank and there is a large residual of LH_2 in each tank at MECO. However, N_2 has been assumed since this would permit the astronauts to work in a shirtsleeve environment provided the pressure was temporarily raised. CO_2 is also a possibility and has the advantage that, being stored as a liquid, it would be handled at a lower pressure than N_2. O_2 is also readily available on-orbit from the O_2 tank and unlike N_2, the astronauts could work in the tank without requiring portable oxygen units. Whatever gas is used it will be necessary to know its composition and density, i.e., its pressure and temperatures.

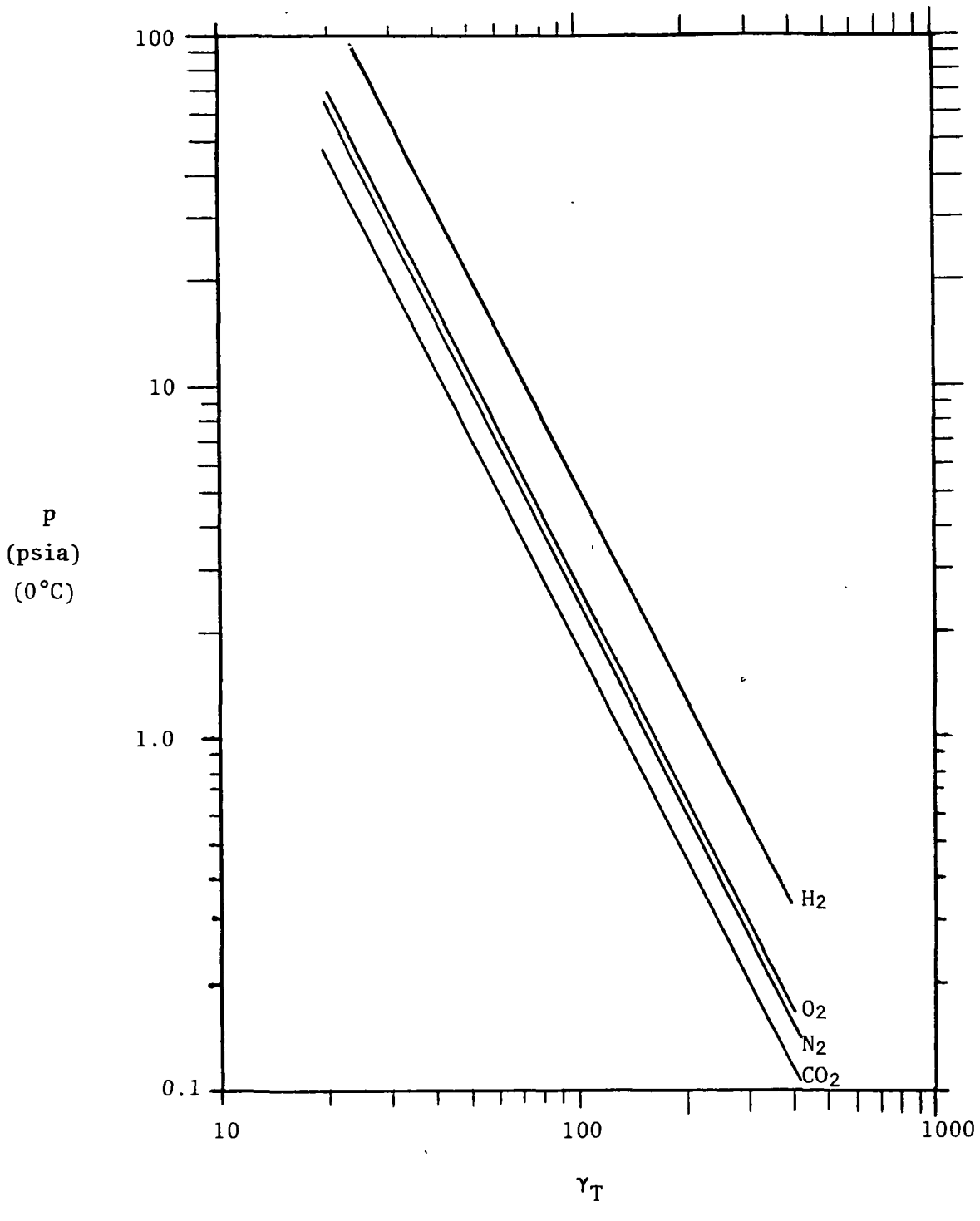

Figure 8. Pressure, p, for various gases vs. the selected threshold Lorentz factor, γ_T.

3.8 Immunity to Background Cosmic Rays

ONE OF THE GREAT VIRTUES OF THIS TELESCOPE IN ADDITION TO ITS SIMPLICITY AND LARGE APERTURE IS ITS INHERENT ABILITY TO NATURALLY REJECT VIRTUALLY ALL NON-GAMMA-RAY EVENTS. What follows is a litany of potential background events and a description of how each is rejected.

3.8.1 Direct Registration of Primary Protons

The expected number of events of this type is

$$N_p = I_p A t d \Omega (1 - \varepsilon_A) \varepsilon_1^2 \varepsilon_2 \qquad (30)$$

where ε_A is the efficiency of the veto scintillator, S1 $\gtrsim$99%, and ε_1 is the probability that the pulses in S2 and S3 due to a single charged particle exceed the threshold detection level set for a pair, $\lesssim$1%. ε_2 is the probability of a single charged particle producing the same amount of light as a pair of particles. Two particles will generate on the average 60 photoelectrons. If the threshold for detection is set at 48, the probability of detection is 0.935. The probability of a single particle producing 48 or more when 30 is expected is 0.0014. The probability of accepting one particle when two are expected is then $\varepsilon_2 = 1.5 \times 10^{-3}$. I_p is the proton flux above the energy required for Cherenkov-light production in the gas, namely about 100 GeV. This flux is about $10^{-3} cm^{-2} sec^{-1} sr^{-1}$. The remaining parameters are as in (12). Production of the light via knock-on electronics from protons of lower energy adds only about 10% to the rate. Taking the integral diffuse gamma-ray flux for high galactic latitudes above 250 MeV to

be 2 x 10^{-5} photons/cm^2/sec/sr, (Mayer-Hasselwander, et al., 1982) then gives

$$\frac{N_p}{N_D} = \frac{I_p\,(1 - \epsilon_A)\,\epsilon_1^2\,\epsilon_2}{\alpha\, I_D\, \epsilon_c} \approx 2.6 \times 10^{-6} \qquad (31)$$

Thus the rate of primary proton detection is small in comparison to the diffuse gamma-ray background.

3.8.2 Protons Interacting to Produce Pions

The threshold energy for charged pions to produce Cherenkov light is lower, 15 GeV, than for protons. However, the energy of the primary proton necessary to produce the pion must still be above 100 GeV. Since the converter plus scintillator amount to only 1/60 of an interaction length, this process is negligible compared to direct registration of primary protons. Protons will also interact, producing neutral pions which immediately decay to produce a pair of gamma-rays. These gamma-rays will be detected in the same way as primary gammas. However, on the average they will have only half as much converter in which to pair produce. Finally, the Cherenkov light produced by all the secondaries from the proton interaction must not mimic that produced by just a single pair. Thus it is even less likely to detect the products of proton interactions than to detect protons directly.

3.8.3 Muons

Muons that stop in the converter and subsequently decay have been troublesome in some detectors because the decay electron originates on the average 2.2 microseconds after the muon signal and can appear to have been generated in the converter by neutral

radiation. To avoid these spurious events the use of a long veto pulse (about 10 microsec) is generally required. This would rule out the possibility of constructing an apparatus on a large scale (because of jamming). The gas-Cherenkov telescope avoids this problem. The high threshold energy for producing Cherenkov radiation makes this instrument completely insensitive to the decay electrons of stopped muons. Thus, the veto pulse width can be kept extremely short, on the order of 5 nsec, and a large area is possible without jamming. Additionally, a gamma-ray burst producing a high instantaneous count rate in excess of many megahertz can be recorded .

3.8.4 Backward-Going Particles that Stop in the Converter

Backward-going particles, which stop in the converter and hence fail to trip the veto scintillator, could look like electrons produced by gamma-rays in the converter. The gas-Cherenkov telescope is insensitive to these events for several reasons:

1. Any Cherenkov light that may be produced by backward-going particles can reach the phototubes only if the particle itself passes through the focal plane.
2. The threefold time-delayed coincidence of the pulses between the Cherenkov light-collecting phototubes and in the scintillators would be incorrect.
3. The light reaching the focal plane will be in the form of a pool of 1.4 degrees diameter rather than a ring resulting from the imaging of the mirror.

3.8.5 Primary Electrons

Through inefficiency of the anticoincidence scintillator, electrons might be recorded as spurious gamma-rays in the same way that the fast protons could. Although primary cosmic-ray electrons are much less numerous than are protons of the same energy, the threshold energy for electrons to radiate is much lower than for protons. This lower value for electrons is due to the threshold energy of this detector depending on the Lorentz factor. Above the approximate threshold of 90 MeV for a single particle, the electron flux in space is $0.166/cm^2/sec/sr$ (Hayakawa, p. 632, 1969). This value is 166 times greater than the flux of protons above the Cherenkov threshold. Comparing the electron background with that of diffuse gamma-rays, the ratio is about 166 times that given by (31), i.e.,

$$\frac{N_e}{N_D} \lesssim 4.3 \times 10^{-4} \qquad (32)$$

3.8.6 Chance Coincidences

A chance coincidence requires a pulse in the pair-recording scintillator S2, unaccompanied by one in the veto scintillator S1, followed after 79 nsec by an unrelated pulse in S3, and followed after an additional 13 nsec by an unrelated pulse of the correct amplitude in Cherenkov light-collecting phototubes. The pulses in S2 unassociated with veto pulses in S1 will be due mainly to soft electrons entering from below and to gamma-rays outside the acceptance angle of the telescope. The estimated pulse rate is 2×10^4/sec. The pulse rate in S3 is expected to be about 4×10^5/sec. The pulse rate in the focal plane will be dominated by

Cherenkov pulses from primary electrons hitting the focal plane. This rate is

$$R_{FP} = I_e A_2 \Omega_2 \varepsilon_2 = 1.1/\text{sec} \qquad (33)$$

where

I_e = .166 electrons/cm^2 sec sr

$A_2 \simeq 5.9 \times 10^3 \text{cm}^2$,

$\Omega_2 = \pi/4$ sr (30°FOV, since an electron from a steep angle will produce substantially less light)

and ε_2 = .0014 as before (Section 3.8.1).

Combining these rates and using a 5-nsec pulse width, Δt, gives a chance coincidence rate of

$$N_C = 4 R_2 R_3 R_{FP} (\Delta t)^2 = 8.8 \times 10^{-7}/\text{sec} . \qquad (34)$$

The diffuse gamma-ray rate above the effective threshold energy is

$$N_D = \alpha I_D A \Omega \varepsilon_C = 7.7 \times 10^{-4}/\text{sec}$$

where α = .97, $I_D = 2 \times 10^{-5}$, A = 2.4×10^5, Ω = .006, and ε_C = .0276 all as used before.

Thus the ratio of chance coincidences to the diffuse gamma-ray background is

$$\frac{N_C}{N_D} \simeq 1.1 \times 10^{-3} \qquad (35)$$

which also can be neglected. The character of the pulse of light has been neglected, i.e., an unimaged cone of light will appear as a filled pool of light rather than a ring. This will reduce

significantly the rate R_{FP} when the images are analyzed.

3.8.7 Summary of Background Effects

The dominant background effect is due to primary electrons, which might be expected since the telescope is designed to detect them as the secondaries produced by the incident gamma-rays. However, the effect of the primary electrons is small compared to the diffuse gamma-ray background. In summary, the non-gamma-ray background is rejected in a natural way by:

1. Requiring a large Lorentz factor
2. Detecting the image and amplitude due to two Cherenkov light cones
3. Tightly packing the converter with a trigger and a veto scintillator, and
4. Requiring a threefold fast time coincidence appropriately delayed for the long time of flight between system components.

Note also that these backgrounds were compared with the diffuse flux at high galactic latitudes. On the plane and especially toward the galactic center the background effects will be somewhat more negligible.

4.0 TELESCOPE-COMPONENT DESCRIPTION

4.1 The Tank

The principal component necessary for this telescope to work, the LH_2 portion of the ET, is the ideal vessel for many reasons. It is large, thin-walled, gas-tight, light-tight, insulated, and rigid. There are no central obscurations and it already has three 36-inch manholes. Finally it is available at no cost (normally it is disposed of) and the energy required to put it in-orbit has already been invested into it. It is truly a windfall to the user.

As described in Section 3.7 the telescope must operate within a pressure vessel at a few psi. The ET is designed to operate up to 40 psi, thus it can be operated safely as a telescope. In addition, the ET operating pressure is not so much greater that the tank wall would significantly absorb the gamma-rays or serve as a source of secondary gamma-rays due to high energy cosmic-ray interactions. Figure 9 is a drawing of the aft dome (front of the telescope) and on it are indicated the typical thicknesses of the aluminum. Assuming an average thickness of 0.12 inches within the field of view, the gamma-ray attenuation is only 2.6% and there is only 1/129 of an interaction length for primary protons to produce pions. Because of these concerns, it is important to maintain the material thickness within the field of view at an absolute minimum. Therefore it is desirable to remove the hydrogen siphon and anti-vortex baffles from the aft dome. According to MMA, it appears to be feasible to do this by unbolting it from the inside and stowing it in the region of the forward dome.

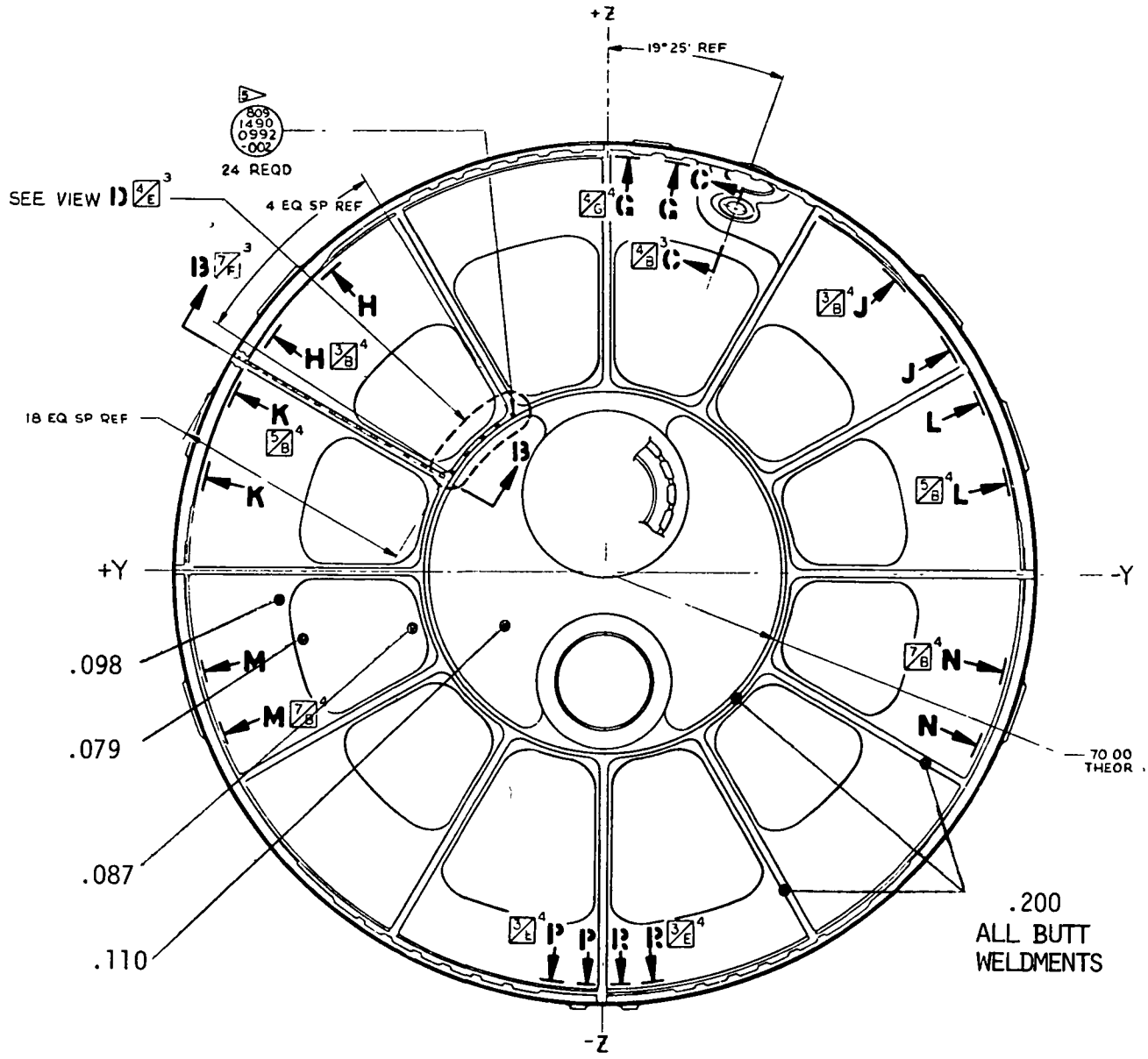

Figure 9. Wall thickness (inches) of aft dome.

4.2 The Trigger Module and Sensitive Area

In order to detect the gamma-rays they are first converted to an electron-positron pair. To be able to determine that this has happened, the converter is surrounded with plastic scintillator. Plastic scintillator has the property that when an energetic charged particle passes through it, it emits a very fast pulse of light, on the order of 5 nsec in duration. The light can be efficiently collected and detected with photomultiplier tubes (PMT). Each scintillator with its PMTs is sealed in aluminum foil to optically isolate it. One layer of scintillator is placed on the incident side of the converter; this is used as a veto to reject all charged particles. The converter used is generally a high Z material to minimize weight. A sheet of lead 0.2 mm thick will provide the necessary radiation thickness. Another scintillator is placed on the exit side to detect the charged pair produced by a gamma-ray. When a pulse indicative of two particles is seen in the trigger without a coincident pulse in the veto, it is very likely that the event was due to a gamma-ray. The trigger scintillator is slightly smaller than the veto to ensure charged primary rejection near the edges. To minimize scattering a scintillator 4 mm thick will be used.

The trigger module is limited in size by the manholes in the ET. Many modules are necessary to define the active area of the telescope. A convenient shape for the modules is hexagonal. Adiabatic light pipes can be attached to two opposite edges, making for fairly uniform and efficient light collection utilizing the property of total internal reflection within the scintillator and

light pipes for conducting the light to the PMTs. To provide mechanical strength to the modules so that they can be handled by the astronauts without fear of breaking, an aluminum honeycomb sandwich is included. The module as described is shown in Figure 10.

These modules and slightly truncated versions of them can be arranged to define the aperture. The clear aperture is limited by the inside diameter of the 2058 ring at the base of the aft dome. This diameter is 252 inches. Although a larger aperture would be desirable, vignetting would result in the gain in off-axis area to be marginally useful. With the present configuration the sensitive area is constant within the field of view. Figure 11 shows the layout that would fill the clear aperture with the modules shown in Figure 10. The areas containing the light pipes and PMTs would be inactive. There is no overlap of the modules in order to minimize the amount of scattering material after the pair is produced. The arrangement of the outer ring has been chosen so as to place light pipes and PMTs at the six corners and thereby minimize the loss of active area. The flat side-to-side dimension of a trigger scintillator is 78 cm and the sensitive area per module is 5270 cm^2 for a whole module and 4172 cm^2 for a truncated module. With 36 whole and 18 truncated modules the total sensitive area will be $2.5 \times 10^5 cm^2$. (Those portions of a module that would be blocked by the 2058 ring would be made of clear plastic.) The large inactive area in the center serves a dual function:

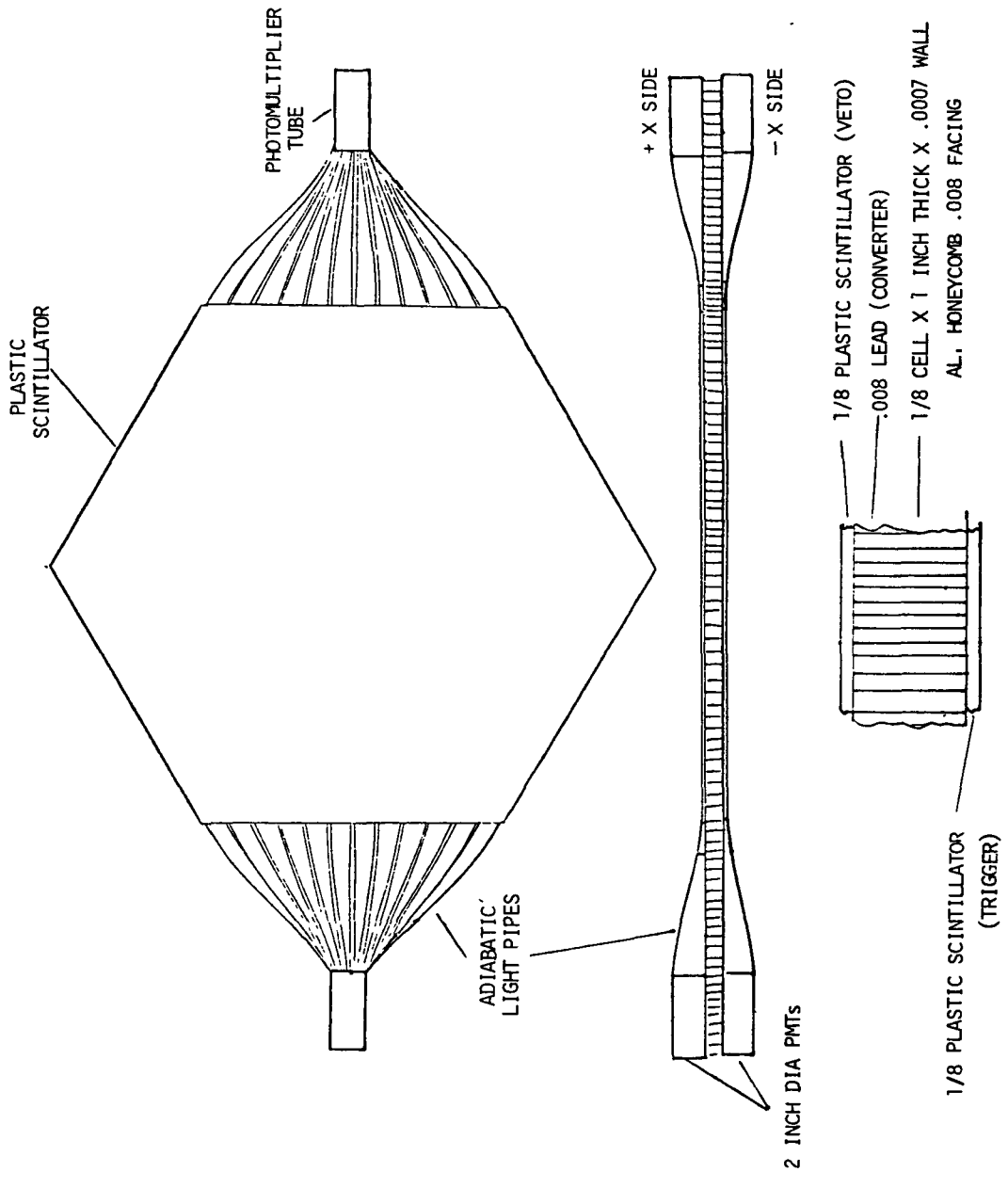

Figure 10. Typical trigger module.

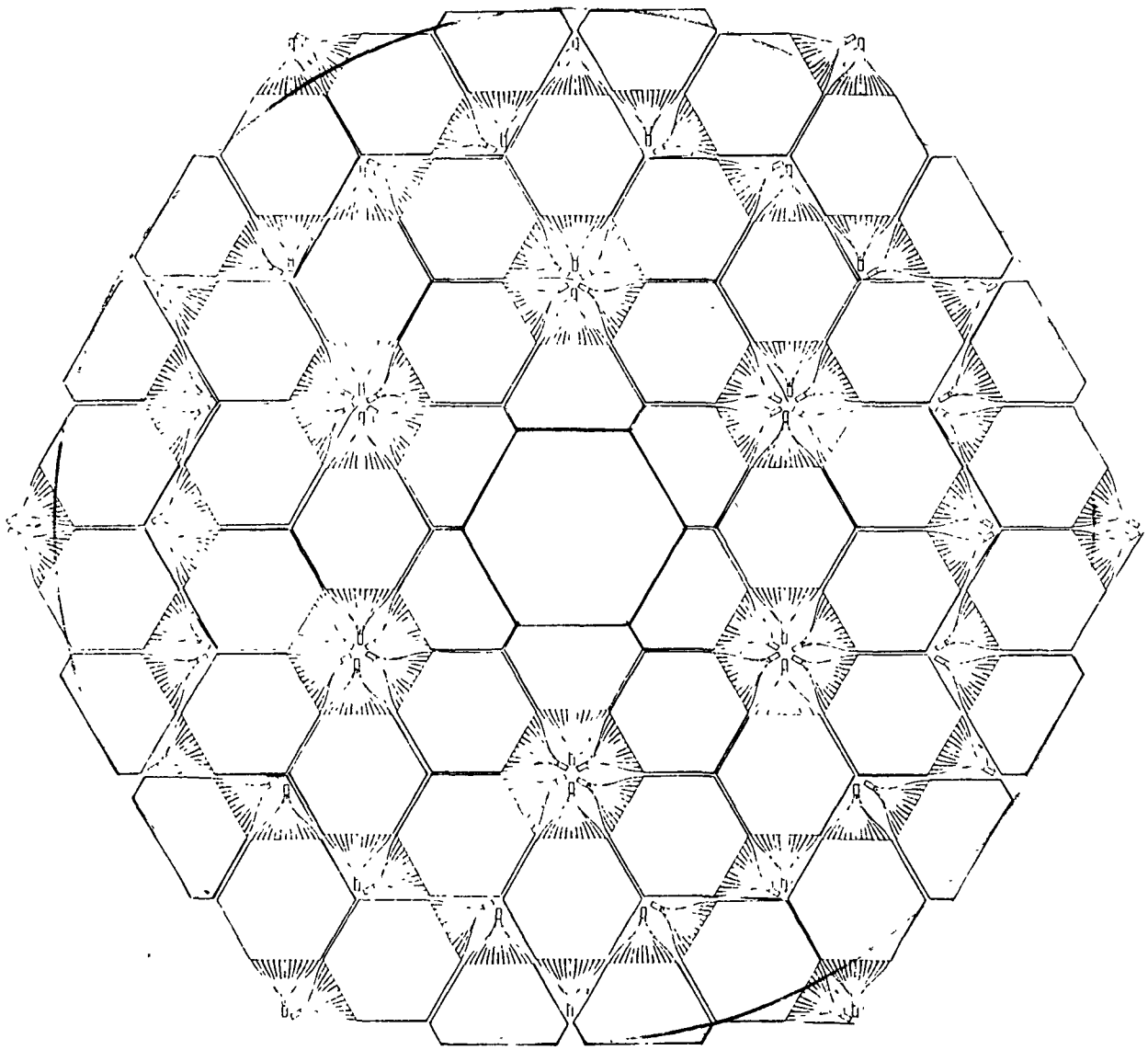

Figure 11. Layout of the trigger module assembly. The 252 inside diameter of the 2058 ring is also shown.

1. To permit astronaut access (45 inch side to side), and
2. The focal-plane array introduces some central obscuration.

Each module would have mounted on it a small electronics module. It would provide the following functions:

1. Receive 28 VDC power and convert it to the necessary 2-3 kV required by the four PMTs. The high voltage connections between the HV supply and the PMTs would be hardwired and potted. No HV connectors would be used.
2. Using emitter-coupled logic (ECL) the module would perform the necessary fast asynchronous logic processing, thus providing the appropriate fast signal via 50-Ohm cable to the central logic unit for all the modules.
3. Permit selection via a coded command one of the following signals to be sent to the central logic unit:
   a. veto scintillator only (for housekeeping health check)
   b. trigger scintillator only (for housekeeping health check)
   c. $\overline{\text{veto}}$·trigger (for master trigger logic)

All of these modules would be protectively packed into a shipping crate and placed in the Orbiter cargo bay. A NASA "standard shipping crate" could be developed for this purpose which would provide a thermally protected, acoustically isolated, and contamination-free environment. The modules would then be removed from the crate and installed by the astronauts, at present a novel way to build a satellite but hopefully the beginning of what should

become commonplace. One great advantage to this approach is that individual modules do not have to be as rugged as similar equipment has had to be in the past, since the protective packing can provide support and isolation from the launch loads.

In the IR&D study done by MMA, a concept was developed for mounting the modules to form the array. This consisted of stretching a fabric across the 2058 ring and attaching the modules with Velcro or push-in pins. The trampoline, as it has come to be called, would have the wiring harness sewn in it and would be rolled up so that it would fit through the manhole. Alignment of the trigger modules on the trampoline is not critical.

4.3 The Mirror

Unlike the previous forms of gamma-ray detectors, this one will function much like a conventional optical telescope in that a mirror is used to collect information over a large area and concentrate it at the focal plane. Since the error in the image reconstruction technique is anticipated to be on the order of 5 arcmin, it is not necessary for the image quality of the mirror to be any better than 1 arcmin. A 311-inch diameter mirror attached at the 1377 ring frame would provide an unvignetted field of view. To include the full cone of light the mirror diameter will be made as large as possible to fit within the 328.5 I.D. of the tank (wall thickness plus stringers).

Two possibilities for the mirror construction were considered, a single element and a segmented multi-element design. If constructed as a single element, it would have to be installed in

the tank during its assembly at Michoud. Its advantage is that it would reduce the amount of on-orbit assembly required. The problems with this concept are:

1. No vendor has been found from which a single mirror of the required size is readily available.
2. The effects on the flow of liquids and gases within the LH_2 tank during launch would probably be unacceptable. In particular, hot GH_2 is entering the top of the tank, while cold LH_2 is being siphoned from the bottom.
3. It is not clear that the quality of the mirror would be acceptable after launch, due to either thermal stress or degradation of its front surface.

For these reasons a segmented design was pursued. High quality segmented mirrors of 10-meter diameter have been built in the past (Fazio, et al., 1968, and Leighton, 1978). In both of these designs, each element was a hexagon. The component array was held together by a lattice framework. In this way a large reflector with the required resolution could be constructed at an affordable cost. Indeed, the mirror used in the prototype version of this telescope was segmented and was literally home spun (out of epoxy) hexagons.

The individual mirror elements would be constrained in size to be less than 36 inches in order to fit through the existing manhole. Figure 12 shows the layout of the proposed array. It would consist of 61 whole segments and 24 truncated ones. Each element would be made out of an aluminum honeycomb sandwich that has a very high strength-to-weight ratio. The backface would have a flat plate bonded to the honeycomb. The front of the honeycomb would be

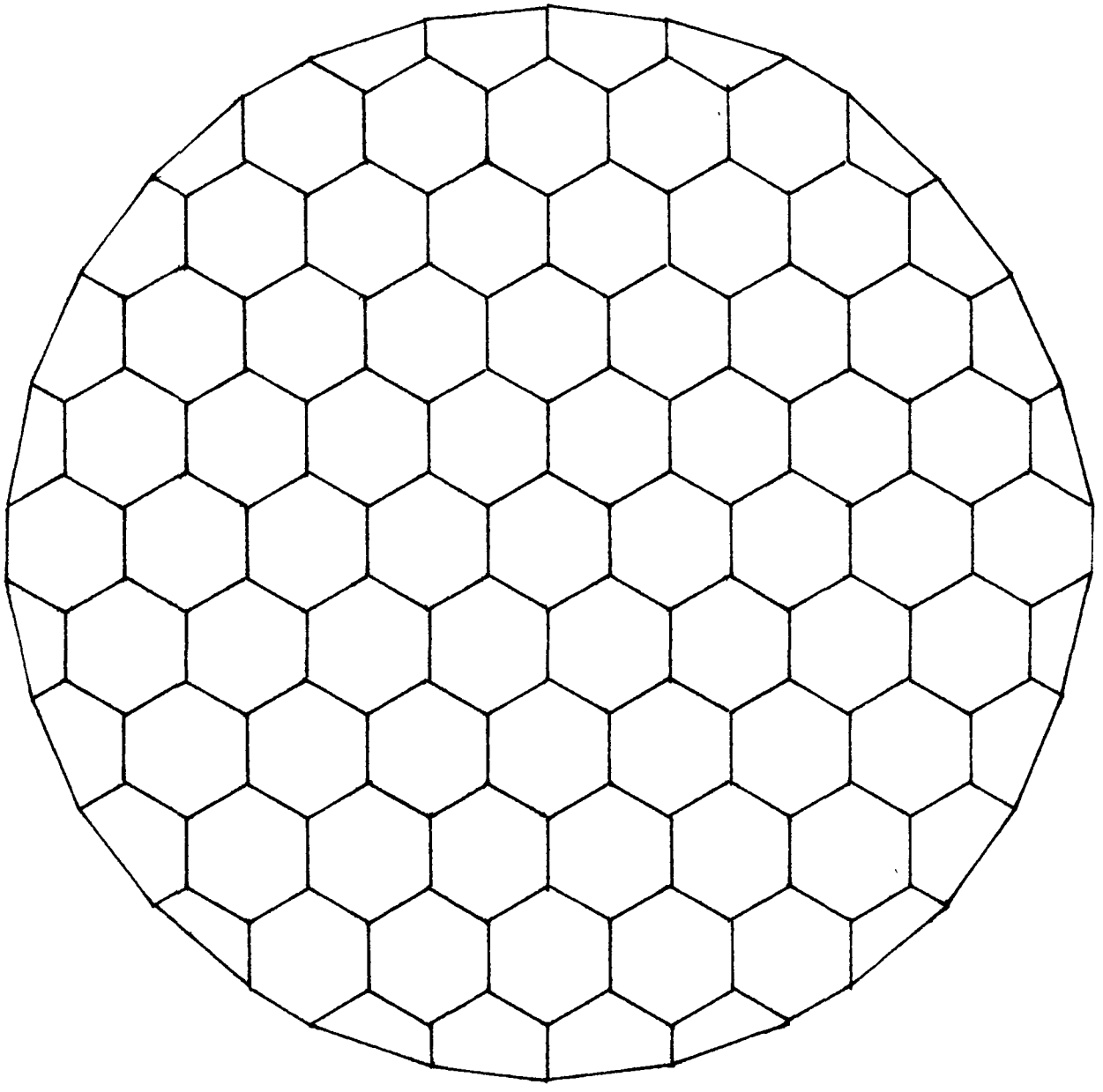

Figure 12. Layout of the segmented mirror. Mirror is 328 inches in diameter and 400 inches in focal length.

roughly machined to the proper curvature. The front plate would be predeformed prior to bonding. Inserts would be incorporated in the sandwich for mounting purposes. The front surface would then be appropriately machined, polished, and coated using conventional techniques. The figure of the mirror would be referenced to the mounting pads so that the elements would be interchangeable, thus simplifying later installation by the astronauts.

The elements would be supported by a lattice framework. The layout of this is shown in Figure 13. It would be made a welded structure of thin-walled aluminum tubing and installed in the ET during assembly at Michoud. From the study carried out by MMA it was concluded that this would be feasible without impacting the qualification of the ET. This is one of only two major modifications to the ET. The lattice design ensures that there are no stresses induced to the mirror segments by requiring all three mounting points for an element to be connected via a triangle. The strength of the structure will be dictated by the launch loads and/or the stiffness under 1 G while performing the original alignment on the ground. The lattice would be mounted to the ET with a three-point mount having the necessary six degrees of freedom since the tank itself becomes elliptical when it is laid on its side and there will be differential thermal expansion during cryogen loading and launch and while on-orbit. The mirror is currently shown as being mounted to the major ring frame at STA 1377; however, the closer it is to the forward dome (back of the telescope), the longer the path length for producing Cherenkov light, which is very critical. Longitudinal struts between the 1130

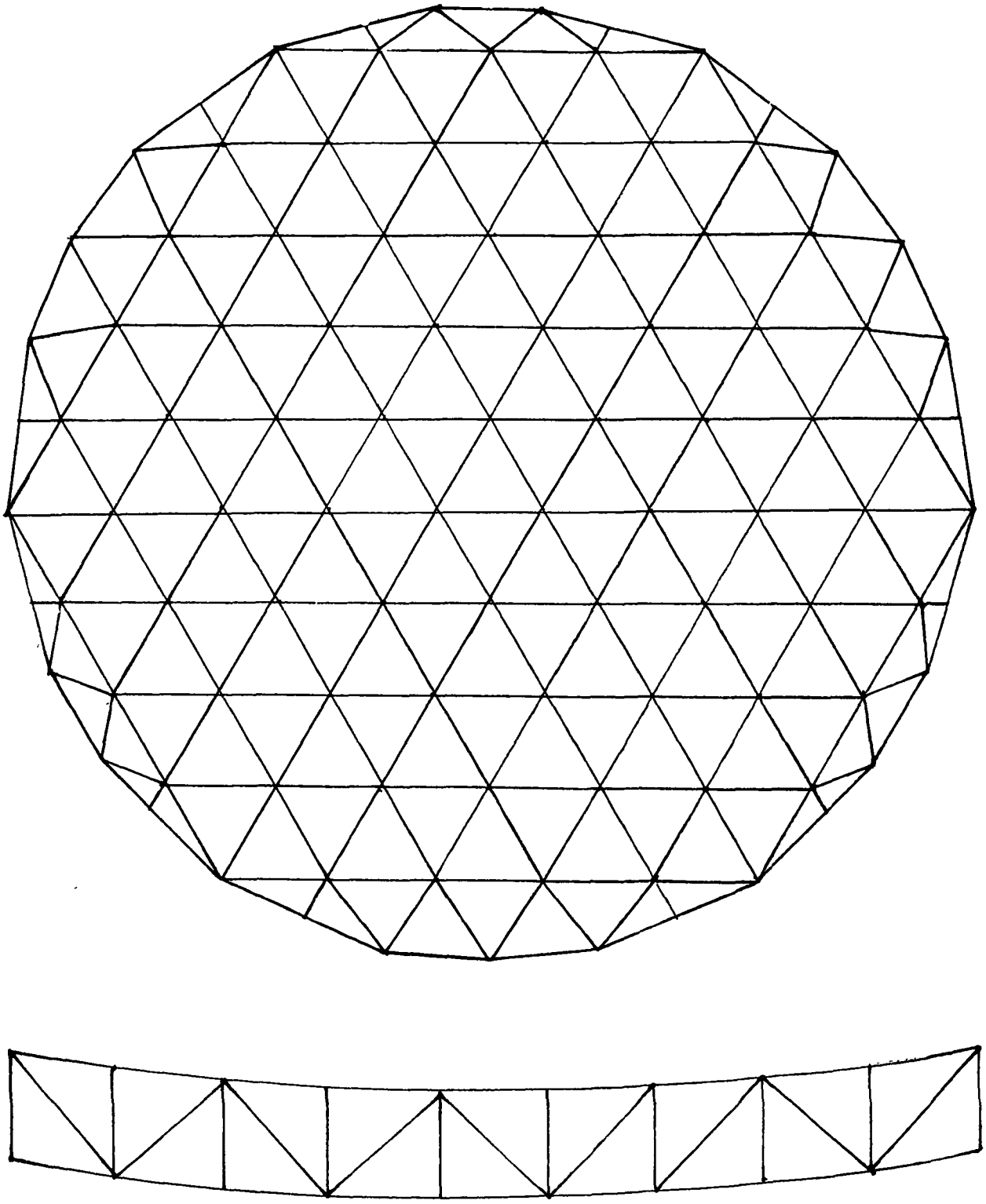

Figure 13. Lattice support structure for segmented mirror. The mirrors are always mounted onto three mutually adjacent nodes.

and 1377 ring frames would permit this as well as distributing the launch loads.

To minimize off-axis distortion, particularly in optical systems with a large field of view, it is desirable to maximize the focal length. It is also desirable to be able to verify the mirror alignment. This would be possible if the focal length were chosen to be equal to half the distance from the mirror to the aft dome, that is, a focal length of 400 inches. Then a point source placed at that point would be reflected back onto itself from all mirror elements. With this focal length and a 5-degree field of view, the focal plane (Figure 3) would be 33.5 inches side to side, just small enough to fit through the manhole.

The mirror elements would initially be aligned on the ground, then packed in shipping crates for delivery on-orbit, and reinstalled by the astronauts. The alignment tolerance of one arcminute allows for a mechanical fit on the mounting pads to within .008 inches, which is well within the realm of reproducibility. Alignment can be verified during installation both on the ground and on-orbit by placing a point light source and TV camera at twice the focal length.

4.4 The Focal Plane

The requirements for the focal-plane detector are that it must have very fast time resolution (a few nanoseconds), have reasonable quantum efficiency, ~ 25%, have good amplitude resolution right down to the single photon level and have enough elements in an array to provide the necessary spatial resolution. Neither image tube nor

solid state cameras can provide the required time resolution. The only device that can fulfill all of the above requirements is a photomultiplier tube (PMT). An array of 127 PMTs has been selected. For a 5-degree FOV the center-to-center tube spacing would be 0.42 degrees. With the 400-inch focal length mirror the plate scale is 1 degree to 6.98 inches or 2.932 inches tube center to center. A particularly good tube type for this application is a 2-inch PMT made by RCA, the 8850. This tube has a bialkali photo cathode with a peak quantum efficiency of about 30% and a GaP first dynode that is of sufficiently high gain to permit single photoelectron resolution. One variant of this tube (the C31000M) has a quartz window that extends the sensitivity to 200 nm where the Cherenkov light is most intense. Another version of this tube (the C31057) is available ruggedized for space flight. All of these features could be made available in one tube.

So that light is not lost between the PMTs, hexagonally-shaped reflective light cones are placed on each tube. Figure 3 shows the focal-plane array. The array would be brought in as an assembled unit and held in place by a tripod which is connected to the mirror fixing it to the optical axis.

The light from each Cherenkov ring will on the average be divided among 14 tubes. By performing pulse height analysis on each tube (at most 4 or 8 levels would be adequate) the rings of light can be reconstructed and the direction of the gamma-ray determined. Off-axis aberrations can be corrected in a unique way, since the trigger module in which the event originated will determine the location within the aperture and hence the amount of aberration that had occurred.

4.5 The Time of Flight (TOF) Module

The time of flight (TOF) scintillator is placed behind the mirror in order to assist in unambiguously identifying each gamma-ray event and in the rejection of non-gamma-ray events. The design of a single module is basically the same as a trigger in that a hexagonally-shaped plastic scintillator is viewed by a pair of PMTs with the light being efficiently transmitted from the scintillators to the PMTs via adiabatic light pipes. The scintillator-light pipe-PMT assembly is wrapped with aluminum foil to optically isolate it. A TOF module will consist of a single scintillator, honeycomb strongback, and electronics module. The electronics module will contain the HV supply for the PMTs and supply a 50-Ohm signal indicative of either one or two electrons formed from the signals from the two phototubes on each module. The modules would be mounted to a trampoline similar to that used to position the trigger modules. Since scattering is unimportant at this time, active scintillator can overlap the light pipes and PMTs and vice versa. In this way all dead areas can be filled with modules. To account for the beam divergence the area of the TOF, like the mirror, must fill the entire cross section of the tank. Figure 14 shows the layout of the TOF modules. The array will consist of 61 whole modules and 24 truncated modules.

If a shower counter were desired in order to obtain greater energy resolution then one or more layers of lead and scintillator would be added to each module. In addition each module would now contain the necessary fast electronics to determine the energy of the shower.

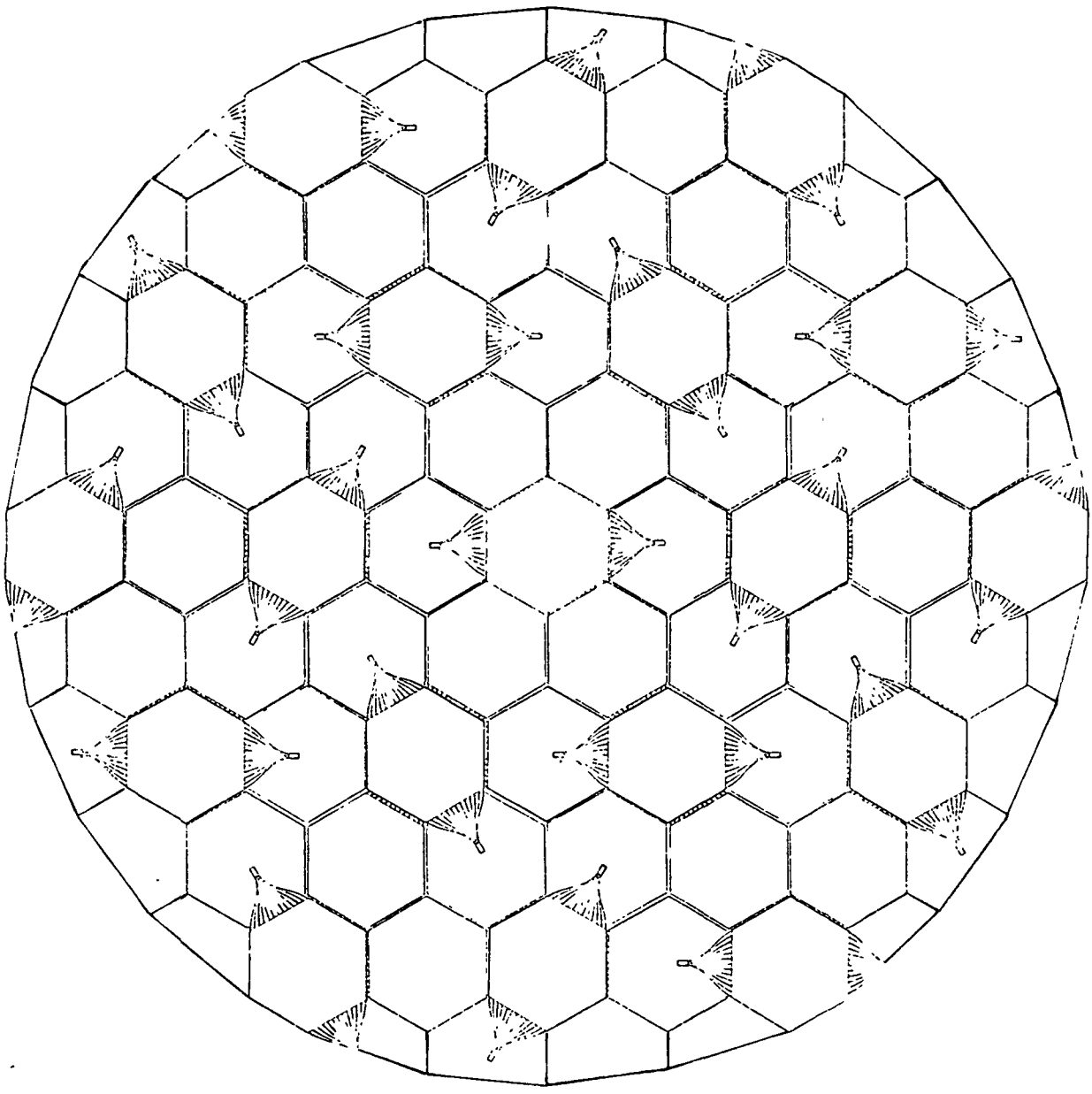

Figure 14. Layout of the time of flight (TOF) scintillator array. The bulk of the light pipes and PMTs have been overlayed by another scintillator to provide a nearly completely active array.

4.6 Telescope Electronics

The ability of this telescope to successfully detect gamma-rays and efficiently reject background relies on the ability to perform time-delayed coincidence between the veto, trigger, TOF, and focal plane. The pulse rise and fall times must be kept to 1 nanosecond and the pulse widths must be no more than 5 nanoseconds. This fast timing can be performed using emitter-coupled logic (ECL). Functional modules are readily available for lab use from a number of commercial vendors (for example, LeCroy Research System, Phillips Scientific, and EG&G Ortec). Literally thousands of these modules are interconnected as part of massive particle detectors at high energy accelerators, cosmic-ray detectors, and the like (Gidal, et al., 1983). What is critical at these high speeds is the design of the interconnection. Exterior to the module, 50-Ohm coaxial cable is required and each connector must be terminated with 50 Ohms to prevent ringing. Likewise the internal design of the module must be done taking into account the capacitance and inductance of every connection. Each path must be considered a transmission line. The point is that the technology exists and it must be used for the telescope to function. In order to achieve the fast switching times, the ECL circuits require higher currents than are normally encountered in logic modules. The power required to operate the telescope will be on the order of 1 kW.

The master event trigger would be generated by

1. Forming a logical OR of all the trigger modules;
2. Forming a logical OR of all the TOF modules;
3. Requiring at least four of the focal-plane PMTs to have two or more photoelectrons; and
4. Performing a threefold properly time-delayed coincidence of 1, 2, and 3.

A master event trigger would then:

1. Latch the pulse height information for all 127 PMTs in the focal plane;
2. Latch the 54 trigger module signals;
3. Latch the clock reading;
4. Latch the attitude reading;
5. Initiate synchronous data readout and recording.

The acid test to prove that the telescope is working is to introduce an incorrect time delay into one of the three coincidence signals. This command capability will be included. Additional capabilities for verifying the health of the telescope will be the monitoring of the background rates in each module and focal-plane PMTs. This can be accomplished as part of the normal housekeeping activity, sampling one module at a time and subcommutating the information.

4.7 Supporting Elements

4.7.1 Attitude Control

Since this is not a surveying instrument, but rather a telescope, it must be pointed inertially, that is, its axes must be held fixed with respect to the celestial sphere. However, unlike a conventional telescope, which requires pointing to a fraction of a resolution element to keep the image on a spectrograph slit or allow for picture taking with a long exposure, this telescope can account for image motion during reconstruction of each event. Thus the pointing requirement is simply to keep the source within about a one-degree deadband of the five-degree field of view. A two-axis system is required as a minimum (pitch and yaw). However, for other reasons, power in particular, three axes may be required. Additionally, the post facto attitude information must be adequate to permit determination to one arcminute. This requirement has been set so that the attitude error does not contribute significantly to the uncertainty in the determination of the gamma-ray direction.

The hold time on any particular source can be anywhere from half an orbit to indefinite. The slew rate need not be rapid, about one degree per minute with a few minutes settling time. This will keep the lost observing time to a few percent, on the average.

There are many possibilities for attitude control but in general no single system is perfect or complete. These include:

1. Reaction wheels which have to be unloaded using another technique.

2. Thrusters which have consumables.
3. Magnetic torquing which cannot be used to control motion azimuthally about the local field direction.
4. Gravity gradient which cannot be used to control motion azimuthally about the local vertical.
5. Spinning the entire spacecraft, but this complicates rendezvousing, power, and telemetry and requires a symetrically balanced mass.
6. Hard mounting, but this assumes the availability of a stable structure with many times the inertia.

Therefore some combination will be required. The most economical and feasible choice will have to be worked out in a Phase B design definition.

4.7.2 Data Acquisition and Telemetry

With the selected converter thickness, the peak count rate is from Vela at about 2 counts/min. The background rate will be on the order of 1 count/min maximum. Thus for planning purposes an average rate not to exceed 5 counts/min will be assumed. The information recorded for each event will include the pulse heights, requiring 512 bytes. The time, attitude, housekeeping, and statuses will not require more than an additional 512 bytes. Thus the total data storage requirement is 7200 Kbytes (57600 Kbits) a day and the data could be dumped in 15 min using an S-band transponder at 64 kbps. For control of the telescope, primarily for pointing, one 64-Kbyte message per day is all that is necessary. For diagnostic purposes, a real-time downlink rate of 1 kbps and command rate of 125 bps are

adequate.

4.7.3 South Atlantic Anomaly Detector

Since the telescope will periodically pass through the South Atlantic Anomaly, and since the telescope has many high voltage devices, the high voltage will have to be turned off to prevent coronal discharge and damage to the power supplies and PMTs. The time at which the power is turned off and on is based on the local ionization rate. A South Atlantic Anomaly Detector will be provided which will consist of a simple windowless Geiger-Müller tube similar to that used on HEAO-2.

4.7.4 Meteoroid Shield

Since this telescope must operate in a pressurized vessel, it is essential to protect the vessel from puncture by meteoroids. This is the same requirement that is faced by a manned Space Station. Development of shielding for the ET would make it even more attractive as a habitat. Fred Whipple (1947) originally suggested a double wall system which is what is now commonly used. The principle being to fragment the meteoroid with an outer bumper spaced sufficiently far from the inner wall for the energy to dissipate. An empirical equation developed by Nysmith (1969) for a double wall aluminum structure giving the relationship of the meteoroid properties and the structural design is

$$v = 0.0029\ (t_1/d_m)^{1.9}(t_2/d_m)^{3.6}(s/d_m)^5\ \text{km/sec}$$

where v is the meteoroid impact velocity in km/sec, t_1 and t_2 are the outer and inner wall thickness, s is the wall separation and d_m

is the diameter of the meteoroid, all in mm. Using t = 0.635 mm (.025 inch) the same as that on Skylab, t_2 = 3.8 mm (for the mean ET cylinder wall thickness) s = 25.4 mm (the SOFI thickness) and v = 20 km/sec, implies that a normal incident meteoroid 2.9 mm in diameter will not penetrate the inner wall. The weight of the shield would be 2500 lbs. to cover the cylindrical portion of the LH_2 tank and 860 lbs. for the aft dome. Since the velocity dependence goes as s^5 and the meteoroid diameter approximately as $s^{1/2}$ great benefit would be derived from increasing s by several inches, i.e., by mounting the shield on standoffs. In addition decreasing t_1 has little effect on d_m but would reduce the shield weight in direct proportion. The intent here is not to design the shield but rather to scope its mass. An optimized shield would result from a Phase B design definition. THIS SHIELD ALONG WITH THE FACTORY INSTALLED-MIRROR ARE THE ONLY TWO MAJOR MODIFICATIONS TO THE ET.

5.0 MISSION SCENARIO*

For purposes of discussion of specific details a mission scenario is presented assuming:

1. The mission would be performed from the Orbiter rather than from the Space Station; and
2. The telescope would be an autonomous free flyer rather than attached to the Space Station.

In any case, a Space Station scenario would not affect the performance of the telescope. Its relation to the Space Station, once assembled, would define the amount of support provided by the Space Station.

For the telescope to be economical, it must not significantly reduce the available resources of a normal STS mission. That is, it must be in the form of a piggyback to a paying mission which will either be deploying free flyers or carrying supplies to the Space Station. This appears quite possible. The estimated weight for all items required for the telescope and its assembly is 7590 lbs. plus 3360 lbs. for a meteoroid shield. This is about one-third the weight of GRO and yet the sensitive area of the telescope is 40 times greater.

The next chapter describes a major modification to the ET that would significantly reduce the work load described in this scenario.

The telescope assembly requires seven crew members for a duration of seven days. Six crew members are assigned to three EVA

*The majority of this chapter is from a Martin Marietta Aerospace IR&D report of work performed by the Advanced Programs group of the Michoud Division done in parallel with this study.

crews of two personnel each. The mission commander is not assigned EVA duties. To create more interior area, the standard Orbiter airlock is moved from its location in the cockpit to an optional location in the Orbiter cargo bay, on top of the tunnel adapter.

The mission timeline includes a three-hour crew member prebreathe requirement. However, by the time this mission is flown, this requirement may be reduced to less than 40 minutes due to equipment and operational modifications.

Prior to launch of the mission, certain modifications are performed on the ET. Among these are the factory installation of the mirror frame, addition of the meteoroid shield, manhole modifications, and various small adapters and flanges to aid on-orbit assembly. Components and equipment used for on-orbit assembly are packaged in the Orbiter cargo bay. When deemed necessary to determine concept feasibility, operational procedures have been amplified and highlighted by indentation. Table 2 provides a summary of the events given in the scenario.

5.1 Detailed Operations

After the launch, the solid rocket boosters (SRBs) are expended and jettisoned. The Shuttle would not undergo the normal maneuver for ET disposal and would continue to use the more efficient main engines for final orbit insertion. After main engine cutoff (MECO), the ET is retained and, at apogee, the first orbital maneuvering system (OMS) burn is initiated, which circularizes the Orbiter/ET. The next two hours are used to prepare for on-orbit operations.

TABLE 2. MISSION TIMELINES

Event Start (Day:Hour:Minute) (Mission Elapsed Time)	Duration (Minutes)	Event	Remarks
		FLIGHT DAY 1	
00:00:00		Launch	
00:00:02.2		SRB Separation	
00:00:08		MECO	
00:00:52		OMS Circularization Burn	Orbit Circularized at 160 NM
00:00:54.7	2 Hours	Post-Insertion Activities	Complete by 00:03:00
00:03:00	15	Prep for ET Venting	
00:03:15	40	ET Venting	
00:03:55	35	IMU Activities	
00:04:30	60	Lunch	
00:05:30	4 Hours	PAM-D Payload Deploy Activities	
00:09:30	35	IMU Activities	
00:10:05	60	Supper	
00:11:05	45	Presleep	
00:11:50	8 Hours	Sleep	
		FLIGHT DAY 2	
00:20:00	3 Hours	Morning Activities (Reduced for EVA Crew #1)	Postsleep, Teleprinter, IMU Align, Breakfast
00:21:30	3 Hours	Prebreathe for EVA	EVA Crew #1
00:22:00	2 Hours	Checkout of SSS & MMU	IVA Crew
01:00:00	1 Hour	Deploy SSS	IVA Crew
01:00:30	3 Hours	Prebreathe for EVA	EVA Crew #2
01:00:30	6 Hours	EVA	EVA Crew #1
01:00:40	20	Don MMUs	EVA Crew #1
01:01:00	1-1/2 Hrs.	Install SSS, Momentum Exchange Devices and Startrackers	EVA Crew #1 & RMS
01:02:00	10	Deploy SSS Solar Arrays	IVA Crew
01:02:30	4 Hours	Remove Aft ET Manhole Cover	EVA Crew #1 (with MMUs)
01:03:00	1 Hour	Lunch	IVA Crew members
01:03:30	6 Hours	EVA	EVA Crew #2
01:03:40	1-1/3 Hrs.	Install Aft Rail Transport System	EVA Crew #2
01:04:00	2-1/2 Hrs.	Checkout of SSS	IVA Crew members
01:05:00	1 Hour	Complete/Recheck SSS, Momentum Exchange Devices and Startrackers	EVA Crew #2
01:06:00	3-1/2 Hrs.	Remove Aft ET Manhole Cover	EVA Crew #2
01:06:30		Terminate EVA	EVA Crew #1
01:09:30		Terminate EVA	EVA Crew #2
01:09:30	9-1/2 Hrs.	Evening Activities	Supper/Debrief/ Rest/Presleep/Sleep

TABLE 2. MISSION TIMELINES (continued)

Event Start (Day:Hour:Minute) (Mission Elapsed Time)	Duration (Minutes)	Event	Remarks
		FLIGHT DAY 3	
01:19:00	3 Hours	Morning Activities	
01:22:00	3 Hours	Prebreathe for EVA	EVA Crew #3
02:00:30	3 Hours	Prebreathe for EVA	EVA Crew #1
02:01:00	6 Hours	EVA	EVA Crew #3
02:01:15	30	Preposition Safety Equipment/MWS	EVA Crew #3
02:01:45	5-1/2 Hrs.	Remove/Store Hydrogen Tank MPS Siphon	EVA Crew #3
02:02:00	1 Hour	Lunch	IVA Crews
02:03:30	6 Hours	EVA	EVA Crew #1
02:03:40	2 Hours	Install Sta 1130 Trampoline	EVA Crew #1
02:05:40	2 Hours	Install Wiring Harness	EVA Crew #1
02:07:00		Terminate EVA	EVA Crew #3
02:07:40	1-3/4 Hrs.	Install Sta 1130 Scintillators	EVA Crew #1
02:09:30		Terminate EVA	EVA Crew #1
02:09:30	9-1/2 Hrs.	Evening Activities	
		FLIGHT DAY 4	
02:19:00	3 Hours	Morning Activities	
02:22:00	3 Hours	Prebreathe for EVA	EVA Crew #2
03:00:30	3 Hours	Prebreathe for EVA	EVA Crew #3
03:01:00	6 Hours	EVA	EVA Crew #2
03:01:15	1-3/4 Hrs.	Preposition Safety Equipment	EVA Crew #2
		Install Sta 1130 Scintillators	EVA Crew #2
03:02:00		Lunch	IVA Crew
03:03:00	4 Hours	Install Mirror Segments	EVA Crew #2
03:03:30	6 Hours	EVA	EVA Crew #3
03:03:40	3-1/3 Hrs.	Install Focal-Plane Array	EVA Crew #3
03:07:00	2-1/2 Hrs.	Mirror Alignment Checks	EVA Crew #3
03:07:00		Terminate EVA	EVA Crew #2
03:09:30		Terminate EVA	EVA Crew #3
03:09:30	9-1/2 Hrs.	Evening Activities	
		FLIGHT DAY 5	
03:19:00	3 Hours	Morning Activities	
03:22:00	3 Hours	Prebreathe for EVA	EVA Crew #1
04:00:30	3 Hours	Prebreathe for EVA	EVA Crew #2
04:01:00	6 Hours	EVA	EVA Crew #1
04:01:15	1-3/4 Hrs.	Preposition Safety Equipment	EVA Crew #1
		Install Sta 2058 Trampoline, Wiring	
04:02:00	1 Hour	Lunch	IVA Crews

TABLE 2: MISSION TIMELINES (continued)

Event Start (Day:Hour:Minute) (Mission Elapsed Time)	Duration (Minutes)	Event	Remarks
04:03:00	2 Hours	Complete Mirror Alignment Checks	EVA Crew #1
04:03:30	6 Hours	EVA	EVA Crew #2
04:03:40	1-1/3 Hrs.	Install Sta 2058 Scintillators	EVA Crew #2
04:05:00	2 Hours	Install MMU Retention Brackets and Handrail	EVA Crew #1
04:05:00	3 Hours	Available EVA Time	EVA Crew #2
04:07:00		Terminate EVA	EVA Crew #1
04:08:00	1-1/2 Hrs.	Stow Aft Rail Transport System	EVA Crew #2
04:09:30		Terminate EVA	EVA Crew #2
04:09:30	11 Hours	Evening Activities	
		FLIGHT DAY 6	
04:19:00	3 Hours	Morning Activities	
04:22:00	3 Hours	Prebreathe for EVA	EVA Crew #3
04:23:00	10	Orbiter/ET Separation	
04:23:10	40	Rendezvous to Station-keeping Position with ET	
05:01:00	6 Hours	EVA	EVA Crew #3
05:01:10	20	Don MMUs	EVA Crew #3
05:01:30	2 Hours	Install E04 Cover Plate	EVA Crew #3
05:03:30	3-1/2 Hrs.	Standby for GRT Activation	EVA Crew #3 & IVA Crew
05:05:30	10 Hours	Evening Activities for Deorbit Crew	Commander & Pilot
05:07:00		Terminate EVA	EVA Crew #3
05:07:30		Evening Activities	Non-Deorbit Crew
		FLIGHT DAY 7	
05:15:30	3 Hours	Morning Activities	
05:18:20	4 Hours	Deorbit Preparations	
05:22:20		Deorbit Burn	
05:23:20		Land KSC	

In addition to these preparations, venting of the ET residual propellants is required. This is accomplished by dumping the residuals overboard through the Orbiter's propellant fill and drain valves. This venting causes an unequal thrust-reaction which is compensated by the Orbiter's RCS.

After ET venting, the inertial measurement unit (IMU) is aligned. One or more PAM-D type payloads may be carried in the Orbiter cargo bay. The crew conducts a predeployment checkout and deploys the payload. Crew presleep and sleep periods complete the first flight crew duty day.

After crew wakeup and morning activities, Crew #1 begins prebreathing for their EVA followed later by Crew #2. Checkout of the telescope support systems saddle (SSS) is conducted by Orbiter cockpit crew members by an analysis of data received through an umbilical from the aft flight deck to the SSS. The Orbiter remote manipulator system (RMS) is activated and checked. The Orbiter RMS grapples the SSS, moves it into view above the overhead aft flight deck observation windows, and commands the SSS legs to deploy. The commands are sent through the Orbiter S-Band data system or an RMS electrical connection.

After nearly three hours of prebreathe activity, Crew #1 enters the airlock, prepares for their EVA, and egresses into the cargo bay. The two manned maneuvering units (MMU) are donned. The RMS moves the SSS over the Orbiter nose where it is placed in the forward SRB thrust fittings. Crew #1 assists in the final placement of the SSS.

Physical connection of the SSS to the ET is made by Crew #1 placing one pin through each forward SRB thrust fitting. A third connection of the SSS is made through a preflight installed special receptacle fitting on the intertank. Electrical power and data bus umbilicals are connected from the SSS to a preflight installed connector. This connector is behind a new preflight-installed access cover on the intertank.

Similarly, an umbilical is connected from the SSS for gas transfer into the hydrogen tank. The gas umbilical is connected to a commandable valve and fitting on the hydrogen tank forward manhole cover. This valve is closed for preflight and launch. The valve is commanded open via the SSS during the on-orbit checkout operations. The power and data umbilicals pass through the modified forward hydrogen tank manhole cover.

The foldup solar arrays are then self-deployed. Checkout of the SSS is completed by the intravehicular activity (IVA) crew in the Orbiter cockpit. The two sets of reaction wheels are attached by the RMS and Crew #1. Similarly, the star tracker assemblies are installed. (At this point, if the ET had to be jettisoned in an emergency, it could function as an autonomous space craft with attitude control. Thus a later rendezvous would be possible.)

Bottles containing the gas to pressurize the hydrogen tank are now connected to the SSS.

Crew #1 will install an EVA rail around the aft manhole of the ET to be used for tank entry, and portable foot restraints are then added to this rail. These are used as an aid for grasping, etc., by EVA crew members. The rails and foot restraints are installed by inserting pins into preflight installed receptor flanges. The rail around the manhole need not be removed as it will be useful for later refurbishment operations. EVA Crew #1 will then remove the ET aft manhole cover.

Special tools are required to remove the 92 bolts that hold the aft manhole cover in place. A zero reaction powered socket wrench, or another suitable wrench, is required. Power is supplied to this wrench via an umbilical from the Orbiter cargo bay. The cover is stored in a receptacle in an Orbiter cargo bay cradle. At this time, the Crew #1 will return to the Orbiter cockpit.

The initial EVA task for Crew #2 is to deploy and assemble the aft rail system. This is used for personnel and cargo transport from the Orbiter and ET aft areas. This aft rail system leads from its cradle in the aft cargo bay to the edge of the tank entry manhole. One end is secured by the cradle while the other is secured by pins to the rail around the manhole. This rail system is jettisonable by Orbiter command to clear the Orbiter in case an emergency separation of the Orbiter and ET is required.

Crew #2 is then available to take over and complete the aft manhole cover removal task if Crew #1 has not completed it. If time permits, Crew #2 may begin prepositioning equipment needed

for the next day's activities and start removal of the LH_2 feedline siphon assembly. Termination of the EVA for Crew #2 and evening activities conclude Flight Day 2.

After morning activities and the prebreathe period, Crew #3 begins their EVA, followed later by Crew #1. The sole objective of Crew #3 is to remove and stow the LH_2 feedline siphon assembly. First, they preposition emergency breathing equipment inside the ET hydrogen tank.

> Referring to Figure 15, the feedline support bracket, item A, is removed. Using an extension bar and socket, the feedline is unbolted at point B. Bolts retaining the 16 vortex baffle support rods (not shown) at points C and D are now removed. The support rods are removed and stowed. The four vortex baffles are unbolted (at points E and F), removed, and stowed.
>
> A pulley system is installed from the aft dome to the forward dome of the hydrogen tank passing through the mirror frame. The feedline siphon assembly is attached to the pulley cord. The siphon support is unbolted (at point G) from the ET aft dome. The feedline assembly is now free to be removed and transported through the mirror frame to the forward dome where it is stowed and removed from the pulley system.

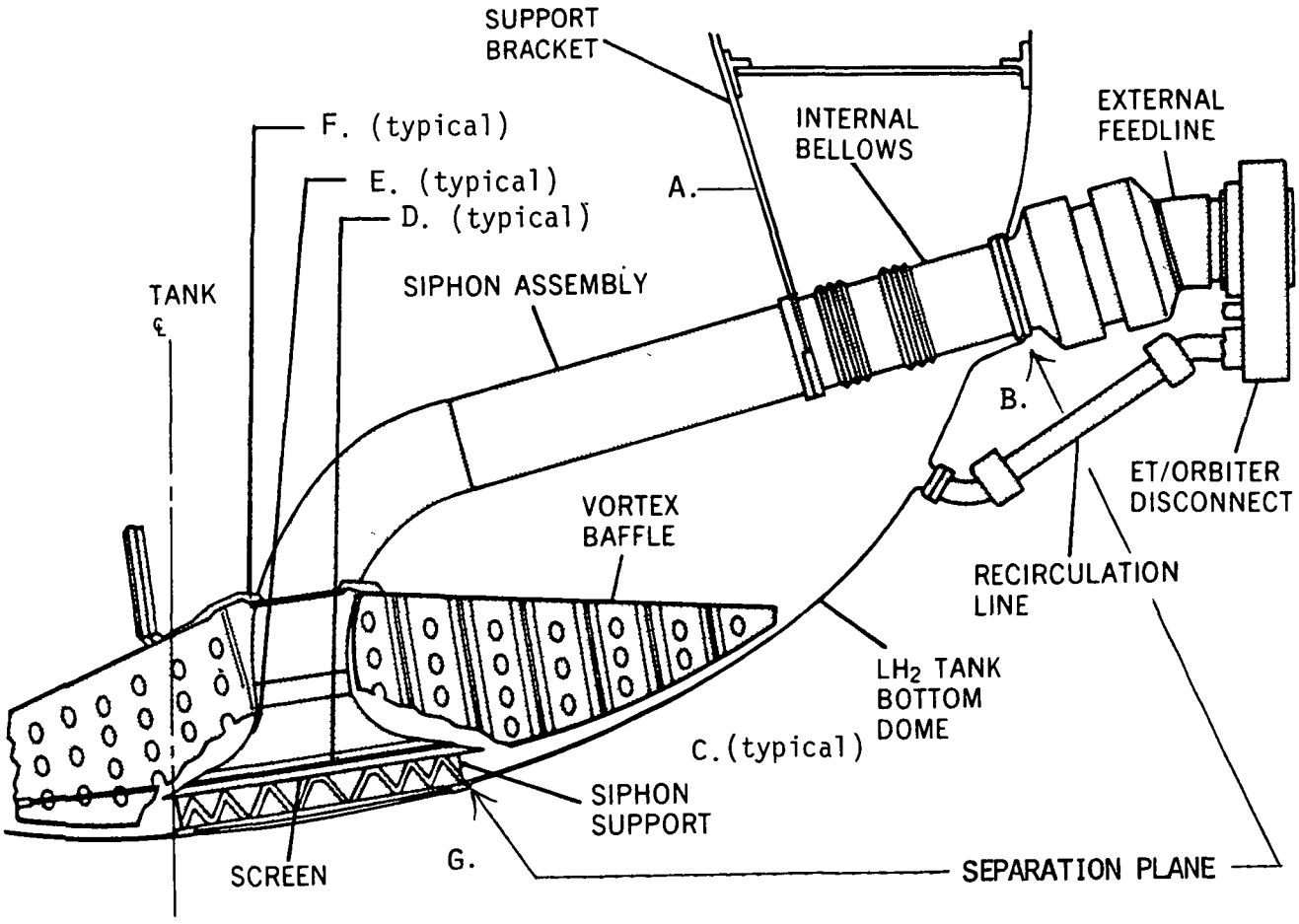

Figure 15. Liquid hydrogen feedline siphon assembly.

This concludes Crew #3 EVA activities for the day.

Crew #1 begins their EVA by removing several extendible poles from the cargo bay. These poles are used as mobile work stations (MWS) inside the ET. Each end of the extendible pole has a rubber-like "foot" for gripping between the stringers of the inside wall of the hydrogen tank. The MWSs are installed just aft of STA 1130 ring frame in the hydrogen tank.

Crew #1 removes the time of flight (TOF) scintillator mounting trampoline from the Orbiter cargo bay and transports it through the open ET manhole, and using the pulley system, to the STA 1130 ring frame of the hydrogen tank. One end of the pulley system is temporarily disconnected. One edge of the trampoline is connected to the STA 1130 ring frame via special preflight installed receptors which are mounted to the ring frame. The crew members then transverse the diameter of the hydrogen tank (along the MWS poles) to attach the opposite end of the trampoline. The trampoline has wiring and connectors already installed and ready to receive the scintillator segments. The MWS poles are moved as necessary to complete trampoline installation. The pulley system is then reinstalled, passing through the mirror frame and trampoline. The pulley system is used as necessary to aid in later personnel and cargo transport.

Crew #1 then removes the wiring harness from the Orbiter cargo bay. The harness is transported to the STA 1130 trampoline where its installation is begun. The harness is secured to the trampoline using Velcro (or other appropriate means) and is plugged into its mating connector. Another mating connector to

the harness is in a protective container and is wired through the hydrogen tank forward manhole cover electrical feed-through fitting. The harness is secured to the interior of the aft dome and sides of the ET as necessary. The harness has a second branch which leads to the STA 2058 scintillator trampoline. A third branch of the harness leads to the focal-plane array, all of which are installed later.

Checkout of the scintillator segments is accomplished by scientists on the ground by data analysis of the downlinked telemetry, during the time period since Orbiter arrival on-orbit. Sufficient spares would be included to permit installation of a fully operational complement of modules. The scintillator segments are packaged in "shipping and testing crates." Each crate stores several segments and each segment has its own electrical connection to an umbilical leading to the aft flight deck. Each crate is also designed to absorb the launch loads and protect the scintillator segments.

After harness installation, Crew #1 begins transporting the TOF scintillator segments from their crates for installation on the STA 1130 trampoline. Each scintillator is attached to the trampoline using push-in pins. Its connector is then plugged into a mating connector on the trampoline. Completion of scintillator mounting should complete the EVA for Crew #1. Evening activities conclude Flight Day 3.

After Flight Day 4 morning activities, Crew #2 completes their prebreathe and commences their EVA (followed later by EVA Crew #3). Crew #2 will transport safety equipment as necessary and complete installation of the STA 1130 scintillators if

required. Crew #2 then begins transporting and installing the mirror segments on the STA 1377 mirror frame.

Each mirror segment is numbered to identify its specific position on the mirror frame. The astronauts use the numbers to assure proper location and orientation of each segment. Each segment is installed from the aft side of the mirror frame. The mirror segment is centered to the mirror frame and connected by springs with a hook to the mirror frame. A point light source and TV camera placed at twice the focal length will be used to verify alignment. Completion of this task should terminate EVA for Crew #2.

Crew #3 begins their EVA by transporting and installing the focal-plane array and tripod mount. The tripod is composed of three legs which are pinned to the mirror periphery (preflight) and to the focal-plane array (on-orbit). The array is composed of 127 PMTs and reflecting light cones. The wiring umbilical is attached and runs along one tripod and then to the main wiring harness. After a total of six hours, the EVA is terminated. Evening activities conclude Flight Day 4.

After Day 5 morning activities and the prebreathe period, Crew #1 begins EVA. They preposition safety equipment and install the STA 2058 trampoline and wiring. The last two hours of their EVA is dedicated to "pin on" installation of two MMU retention bracket assemblies to the aft hydrogen tank exterior. This allows future EVA crew members to approach the telescope and park their MMU prior to tank entry. They also install an EVA handrail from each MMU bracket assembly to the manhole rail.

Crew #2 is the second EVA crew for Flight Day 5. They install the STA 2058 scintillator segments. The installation of the scintillators and wiring is identical to that for STA 1130.

After scintillator installation, Crew #2 is available for 3 hours to perform any unscheduled requirements. After equipment stowage in the hydrogen tank, the hydrogen tank aft hatch is closed. This hatch is installed preflight. To maintain a conservative scenario, the current externally-mounted manhole cover is retained. The aft rail system is stowed in its Orbiter cargo bay cradle. This completes the EVA for Crew #2. Evening activities conclude Flight Day 5.

Flight Day 6 is characterized by the Orbiter/ET separation, followed by an Orbiter rendezvous with the ET. Day 6 will provide time for any contingency activity. Crew #3 will begin their EVA, don the MMU's, fly to the ET, and install cover plates (with gasket) on the 17-inch feedline on umbilical plate E04, the LH_2 recirculation line, and GH_2 pressurization line. Repressurization will begin at this point. They then stationkeep with the ET while the telescope is activated and checked. This completes their EVA tasks.

Meanwhile, the mission commander and pilot begin an early sleep period to allow early wakeup for the next day's deorbit and landing activities. This concludes Flight Day 6 activities.

Flight Day 7 is allocated for standard deorbit day activities.

In summary, the telescope can be assembled in space within four days of a nominal seven-day mission. This mission would include typical payload deployment prior to commencing assembly

activities. The scenario presented has included comfortable margins for contingency activities. This scenario has assumed carrying out assembly from the Orbiter. A similar scenario could be constructed wherein the Orbiter delivered the ET and telescope components and the assembly would be carried out with the Space Station as the base of operation.

6.0 ADVANTAGES OF PURSUING OPTIONS

All of the discussions that have been made so far have been based on the premise that there is to be no redesign or requalification necessary to any of the existing hardware systems. The only significant addition has been inclusion of the mirror lattice in and meteoroid shield on the ET. However, there are a number of options that would provide significant savings in on-orbit assembly time and have applications for other uses, once developed.

6.1 A Side-Mounted Docking Adapter

It is proposed that one of the many side panels that are machined and welded to make up the ET be modified to permit installation on-orbit of a docking adapter/airlock. The new side manhole would be made large enough to permit bringing the various components into the ET in quantity. The RMS would be used to remove the "shipping" crates from the Orbiter payload bay and insert them through the new hole in the ET. An EVA crew would them permanently stow them around the wall behind the 2058 ring and the mirror where they would be out of the field of view. The RMS and an EVA crew would then install the docking adapter/airlock on the side of the ET. After completion of these tasks and return of the EVA crew, the Orbiter separates from the ET and performs proximity maneuvers to dock with the ET. The ET hydrogen tank is then pressurized. Crew members may then move from the Orbiter cockpit through its docking module (JSC 07700, Vol. XIV, Section 9.1.3) through the docking adapter and into the ET.

If the ET pressure is increased to approximately 10 psia for the assembly operations, a modified shirtsleeve environment exists. Crew members will require portable oxygen breathing systems. However, they would not require their standard spacesuit. Crew members would then not have the manual dexterity limitations of spacesuits and assembly operations could become more rapid and perhaps more accurate. In all, the on-orbit assembly time would be significantly reduced. Additionally, since the EVA prebreathe requirement should not exist at all, five to six crew members (vs. two) could assist in the assembly operations each day after the Orbiter docking. Even 24-hour-per-day assembly operations might be possible.

The capability to add a docking adapter to the hydrogen tank could be quite useful in other projects where on-orbit manned entry into the hydrogen tank is anticipated. For example, an empty ET could be docked to a Space Station to increase the internal volume of the station.

The prime motivation from the standpoint of the telescope design is that the component size would not be limited to fitting through the existing 36-inch diameter manholes. Thus there would be fewer pieces to install, fewer electronics modules that could fail, and lower power consumption due to fewer detector modules and processing electronics modules. Table 3 provides a detailed list of the number of components comparing the two situations. The existing manhole requires about 50% more modules and phototubes than use of the docking adapter would require. The scintillators are taken to be 40 inches across which would permit replacement of any failed units by bringing individual ones

through the 40-inch D-hole in the docking adapter.

Table 3
Comparison in the Number of Components.
The two cases are for the existing 36-inch manhole
and the proposed 40-inch docking adapter

	36" Manhole	40" Docking Adapter
Scintillators Required		
Veto	54	30
Trigger	54	30
TOF	85	61
Total	193	121
Phototubes Required		
Veto	96	54
Trigger	96	54
TOF	146	116
Total	338	224
Modules to Install		
Trigger	54	30
TOF	85	61
Mirrors	85	61
Total	224	152

6.2 Aft Cargo Carrier

One of the upgrades that has been proposed for the Shuttle is the aft cargo carrier (ACC), a unit which would be attached to the bottom of the ET. The prime motivation for the ACC is to provide the capability to place into orbit structures that could not presently fit into the Orbiter payload bay. The principal motivation for using the ACC as part of this mission is that all of the support systems would be built into the ACC rather than require on-orbit installation. Secondly, all components would be housed in the ACC, eliminating any use of space in the Orbiter payload bay.

Figure 16 depicts an ACC used to contain the support systems required. This option has another advantage. Should an emergency arise while on-orbit, the ET may be jettisoned at almost any time. This still leaves the ET in a mode which is remotely commandable and capable of subsequent attitude and reboost control without a revisit by an EVA crew.

The support systems and telescope components in the ACC are protected thermally and from meteoroids by the ACC structural design itself. This design allows easy and spacious access by EVA crews. The special aft closure of this ACC has a built-in easily opened manhole hatch. All internal support equipment is located around the periphery of the ACC, which is outside of the telescope field of view. Components and equipment to be used in the construction of the telescope are packaged in the central areas of the ACC since they will be removed and installed in the ET hydrogen tank. This packaging concept shortens both the distance and time required for their on-orbit transferral into the hydrogen tank. Umbilicals for power, data, and pressurization would pass through a special replacement manhole cover. This replacement cover is installed on-orbit.

6.3 Intertank Mounting of Support Systems

Another option that would be advantageous would be to mount all of the supporting systems in the intertank region. Like the ACC it would eliminate a considerable amount of on-orbit assembly and not use up precious Orbiter payload bay volume; however, it would not depend on the development of the ACC or have a weight

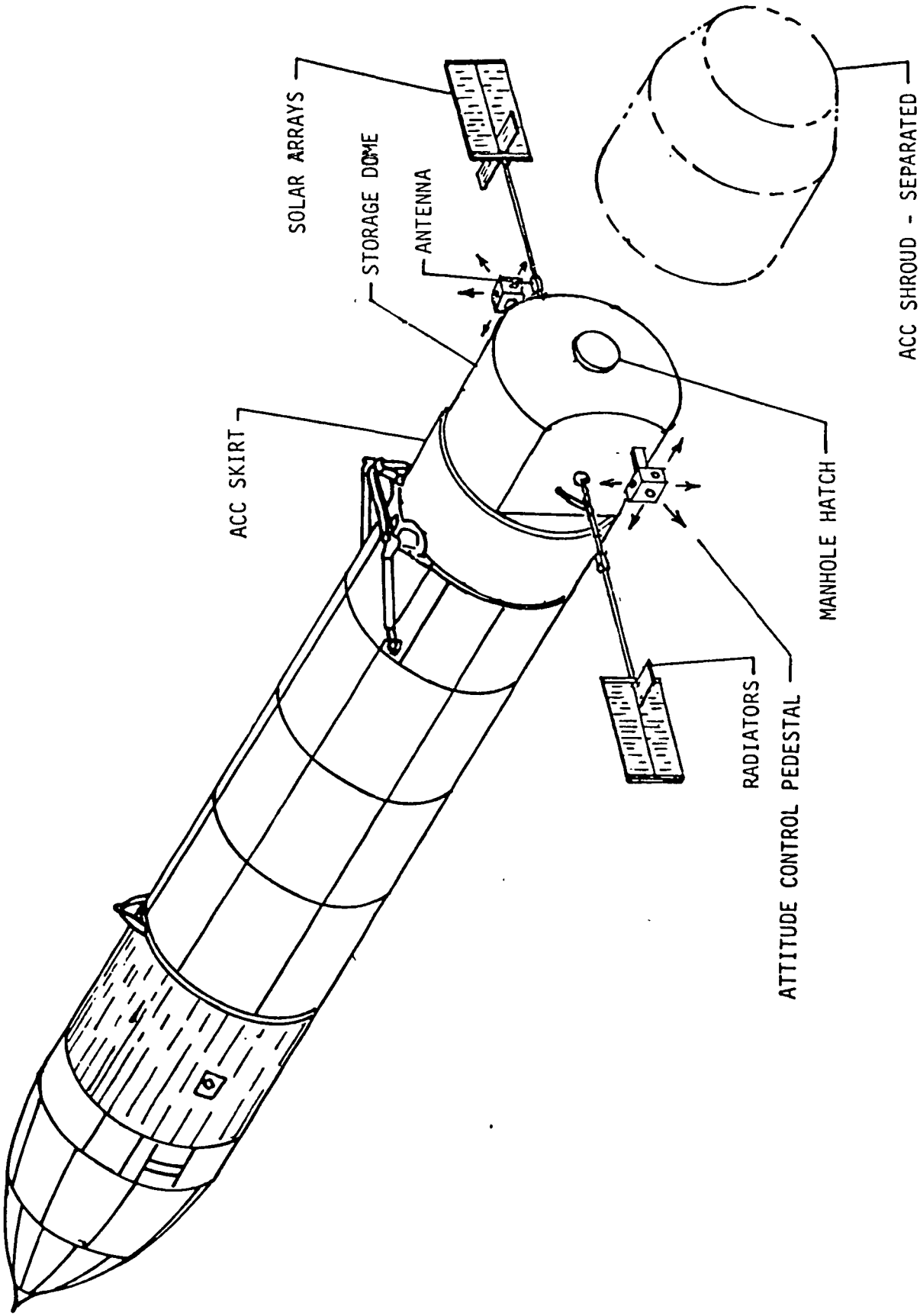

Figure 16. Telescope with aft cargo carrier.

penalty. Like the ACC it would provide meteoroid and thermal protection. It has other features in that reaction wheels or magnetic torquers could be located much closer to the center of mass.

There are a number of drawbacks to using the intertank region. First, the ACC would be a much more universal piece of hardware; and second, access for refurbishment would be more difficult compared to external mounting or ACC mounting. However, the existing doors on the intertank could be configured for on-orbit opening.

7.0 A SYNERGETIC OPPORTUNITY

Converting the ET into a gamma-ray telescope provides the opportunity not only to make a substantial contribution to astronomy, but in addition to make direct use of the ET and demonstrate the feasibility of many of the components that could be applied to future use of the ET as part of the Space Station orbital elements.

Three of the support services required for the telescope and the future Space Station are attitude stability, reboost, and energy storage. A common system solution to all of these is an electrodynamic tether. The concept of an Alfvén propulsion engine was first described by Drell, et al. (1965) and applied to scientific uses with a tether by Colombo, et al. (1974). In a recent article by Bekey (1983), the present understanding of the capabilities of tethered systems is summarized. An electrodynamic tether would provide the three aforementioned support services and its use with this telescope would demonstrate its feasibility for use with the Space Station. An additional feature of Alfvén propulsion is that there are no effluents. Although this is not a problem with this telescope, other telescopes that might be part of the Space Station complement are quite sensitive to contamination, specifically infrared telescopes and coronagraphs.

If magnetic torquing were combined with a gravity gradient system and Alfvén propulsion used for reboost, the entire system would be devoid of consumables. Thus a 5- to 10-year lifetime would depend solely on component reliability.

8.0 CONCLUSIONS AND RECOMMENDATIONS

As a result of this concept definition and the IR&D work performed in parallel at MMA a number of very clear conclusions have been drawn.

1. The ET is an exceptionally well suited resource for conversion into a gamma-ray telescope. It is ideal; fulfilling the need for a large, rigid, light-tight, gas-tight, thin-walled pressure vessel.
2. This gamma-ray telescope will provide the substantial increase in collecting area as recommended by the National Academy of Sciences. This capability is unavailable outside of NASA.
3. A mission flown to deploy this telescope does not substantially reduce the primary function of the mission of delivering a payload to orbit. However, the contribution to astrophysics alone would be justification for a dedicated mission.
4. The support systems developed for this application can be directly applied to other ET applications and Space Station systems, particularly if the ET is incorporated within the Space Station orbital elements. Or vice versa, many of the systems developed for a Space Station can be used to support ET applications.
5. Final assembly of a large instrument on-orbit will pioneer:

1. A new role for man in space; and
2. A new, simpler and less rugged component design concept in which the pieces would be packed rather than integrally strengthened to survive launch.

These techniques will apply directly to the requirements for the Large Deployable Reflector (LDR), an astronomical telescope planned for the 1990's.

Since the External Tank is a valuable resource which can be put to many uses in space, in particular the application described herein:

IT IS RECOMMENDED THAT THE SPACE STATION BE CAPABLE OF SUPPORTING THIS AND OTHER TYPES OF ET APPLICATIONS.

Since the application described herein will provide "an advanced high energy gamma-ray telescope of very large area, high sensitivity and high angular resolution" as recommended by the National Academy of Sciences:

IT IS FURTHER RECOMMENDED THAT NASA PROCEED AT THIS TIME WITH A DESIGN DEFINITION LEADING TO THE DEPLOYMENT OF A LARGE-AREA GAMMA-RAY IMAGING TELESCOPE SYSTEM BASED UPON THE USE OF THE PRESENTLY DISPOSED-OF ET.

This design definition will need to address many of the tradeoffs identified in this concept definition along with those system elements which will be common with and services which will be provided by the Space Station.

Since it will be critical to all ET applications to demonstrate the ability to orbit an ET and it will be economically beneficial to be able to determine by what amount the insulation

on the ET may be reduced

IT IS FURTHER RECOMMENDED THAT AN ET BE TAKEN TO ORBIT IN THE NEAR TERM.

Finally, since there are many possible applications for the ET where meteoroid protection is necessary, including use of the ET as a Space Station element

IT IS RECOMMENDED THAT A VERSION OF THE ET BE DEVELOPED WHICH WOULD HAVE A METEOROID SHIELD.

References

Albats, P., Ball, S.E., Jr., Delvaille, J.P., Greisen, K.I., Koch, D.G., McBreen, B., Fazio, G.G., Hearn, D.R., and Helmken, H.F. 1971, A Large Gas Cherenkov Telescope for High Energy Gamma-Ray Astronomy, Nuclear Inst. & Meth., 95, 189.

Bekey, I. 1983, Tethers Open New Space Options, Astron. & Aeron., 21, 32.

Bethe, H.A. 1953, Molière's Theory of Multiple Scattering, Phys. Rev., 89, 1256.

Bignami, G.F., and Hermsen, W. 1983, Galactic Gamma Ray Sources, Ann. Rev. Astron. & Astrophys., 21.

Chupp, E.L. 1976, Gamma Ray Astronomy (Reidel Publishing Co.).

Colombo, G., Gaposchkin, E.M., Grossi, M.D., and Weiffenbach, G.L. September 1974, Shuttle-Borne "Skyhook": A New Tool for Low-Altitude Research, Reports in Geoastronomy, Smithsonian Astrophysical Observatory.

Draft Report on the Utilization of the External Tank of the Space Transportation System. California Space Institute, La Jolla, August 23-27, 1982.

Drell, S.D., Foley, H.M., and Ruderman, M.A. 1965, Drag and Propulsion of Large Satellites in the Ionosphere: An Alfvén Propulsion Engine in Space, JGR, 70, 3131.

Fazio, G.G., Helmken, H.F., Rieke, G.H., and Weekes, T.C. 1968, An Experiment to Search for Discrete Sources of Cosmic Gamma Rays in the 10^{11} to 10^{12} eV Region, Can. J. Phys., 46, S451.

Fichtel, C.E., and Trombka, J.I. 1981, Gamma Ray Astrophysics, NASA SP-453 (U.S. Government Printing Office).

Field, G.B. 1982, Astronomy and Astrophysics for the 1980's, (Washington, D.C.: National Academy Press), Vol. 1, p. 165.

Gidal, G., Armstrong, B., and Rittenberg, A. 1983, Major Detectors in Elementary Particle Physics, LBL-91 Suppl. UC-37, Lawrence Berkeley Laboratory.

Greisen, K.I. 1966, Perspectives in Modern Physics, ed. R. Marshak (New York: Interscience Publishers), p. 355.

Greisen, K. 1971, The Physics of Cosmic X-Ray, -Ray and Particle Sources (Gordon and Breach Science Publishers).

Greisen, K., Ball, S.E., Jr., Campbell, M., Gilman, D., Strickman, M., McBreen, B., and Koch, D. 1975, Change in the High-Energy Radiation from the Crab, Ap. J., 197, 471.

Hartman, R.C., Kniffen, D.A., Thompson, D.J., Fichtel, C.E., Ögelman, H.B., Tümer, T., and Özel, M.E. 1979, Galactic Plane Gamma-Radiation, Ap. J., 230, 597.

Hayakawa, Satio 1969, Cosmic Ray Physics (New York: Wiley-Interscience).

Koch, D.G., Ball, S.E., Jr., Campbell, M., Delvaille, J.P., Greisen, K., McBreen, B., Fazio, G.G., Hearn, D.R., and Helmken, H.F. 1973, Performance of a Gas-Cherenkov Gamma-Ray Telescope, Nuclear Inst. & Meth., 108, 349.

Kraushaar, W.L., Clark, G.W., Garmire, G.P., Borken, R., Higbie, P., Leong, C., and Thorsos, T. 1972, High Energy Cosmic Gamma-Ray Observations from the OSO-3 Satellite, Ap. J., 177, 341.

Leighton, Robert B. 1978, A 10-Meter Telescope for Millimeter and Sub-Millimeter Astronomy, Final Technical Report for NSF Grant AST 73-04908, Calif. Inst. of Tech., Pasadena.

Mayer-Hasselwander, H.A., Bennett, K., Bignami, G.F., Buccheri, R., Caraveo, P.A., Hermsen, W., Kanbach, G., Lebrun, F., Lichti, G.G., Masnou, J.L., Paul, J.A., Pinkau, K., Sacco, B., Scarsi, L., Swanenburg, B.N., and Wills, R.D. 1982, Large-Scale Distribution of Galactic Gamma Radiation Observed by COS-B, A&A, 105, 164.

McBreen, B., Ball, S.E., Jr., Campbell, M., Greisen, K., and Koch, D. 1973, Pulsed High Energy Gamma-Rays from the Crab Nebula, Ap. J., 183, 571.

Morrison, P. 1958, On Gamma Ray Astronomy, Il Nuovo Cimento Ser. X, 7, 858.

Nysmith, C.R. 1969, An Experimental Impact Investigation of Aluminum Double-Sheet Structures, Proc. AIAA Hypervelocity Impact Conf., Paper 69-375, Cincinnati.

Stecker, F.W. 1971, Cosmic Gamma Ray, NASA SP-249 (U.S. Government Printing Office).

Swordy, S.P., L'Heureux, J., Müller, D., and Meyer, P. 1982, Measurements of X-Ray Transition Radiation from Plastic Fibers, Nucl. Inst. & Meth., 193, 591.

Whipple F.L. 1947, Meteorites and Space Travels, Astron. J., 52, 131.

Wills, R.D., Bennett, K., Bignami, G.F., Buccheri, R., Caraveo, P.A., Hermsen, W., Kanbach, G., Masnou, J.L., Mayer-Hasselwander, H.A., Paul, J.A., and Sacco, B. 1982, High-Energy Gamma-Ray Light Curve of the Pulsar PSR0531+21, Nature, 296, 723.